PL-TR-91-2292

COMPARISON BETWEEN IRREGULARITY MOTION AND BULK PLASMA DRIFTSAT HIGH LATITUDES

Robert C. Livingston
Mary A. McCready

SRI International
333 Ravenswood Avenue
Menlo Park, California 94025-3493

October 1991

Final Report
29 July 1988 – 29 October 1991

Phillips Laboratory
Air Force Systems Command
Hanscom Air Force Base, Massachusetts 01731-5000

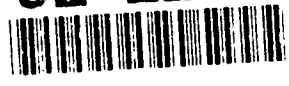

"This technical report has been reviewed and is approved for publication"

SANTIMAY BASU
Contract Manager

JOHN E. RASMUSSEN
Branch Chief

FOR THE COMMANDER

WILLIAM K. VICKERY
Division Director

Qualified requestors may obtain additional copies from the Defense Technical Information Center.

If your address has changed, or if you wish to be removed from the mailing list, or if the addressee is no longer employed by your organization, please notify PL/IMA, Hanscom AFB, MA 01731. This will assist us in maintaining a current mailing list.

Do not return copies of this report unless contractual obligations or notices on a specific document requires that it be returned.

REPORT DOCUMENTATION PAGE

Form Approved
OMB No. 0704-0188

1. AGENCY USE ONLY *(Leave Blank)*	2. REPORT DATE	3. REPORT TYPE AND DATES COVERED
	October 1991	Final (28 July 1988 – 29 October 1991)

4. TITLE AND SUBTITLE
Comparison Between Irregularity Motion and Bulk Plasma Drifts at High Latitudes

5. FUNDING NUMBERS
PE 62101F
PR 4643 TA 08 WU AQ

Contract F19628-88-K-0031

6. AUTHOR(S)
Robert C. Livingston
Mary C. McCready

7. PERFORMING ORGANIZATION NAME(S) AND ADDRESS(ES)
SRI International
333 Ravenswood Avenue
Menlo Park, CA 94025

8. PERFORMING ORGANIZATION REPORT NUMBER

9. SPONSORING/MONITORING AGENCY NAME(S) AND ADDRESS(ES)
Phillips Laboratory
Hanscom AFB, MA 01731-5000

Contract Manager: Santimay Basu/LIS

10. SPONSORING/MONITORING AGENCY REPORT NUMBER
PL-TR-91-2292

11. SUPPLEMENTARY NOTES

12a. DISTRIBUTION/AVAILABILITY STATEMENT
Approved for public release;
Distribution unlimited

12b. DISTRIBUTION CODE

13. ABSTRACT *(Maximum 200 words)*

Coincident measurements of ionospheric motion, derived from two different techniques, are compared. The first technique is incoherent-scatter radar measurement of bulk plasma drift; if the plasma flow is uniform within its field of view, the radar provides precise measurements of motion resolved from multiple line-of-sight velocity samples. The second technique is spaced-receiver measurement of kilometer-scale irregularity motion; the velocity is extracted from the diffraction pattern produced by integrated propagation effects along the radio raypath. Detailed comparisons of coincident measurements are made for five experiments in Alaska and Greenland, under a variety of background conditions. When the ionospheric drifts are uniform, the agreement between the two techniques is good. When this is not the case, as is typical near the polar cap boundary, the superior time and spatial resolution of the scintillation technique reveals small-scale flow patterns which are difficult to derive from the radar data.

14. SUBJECT TERMS
Scintillation; Spaced Receiver; Irregularity Motion; Incoherent Scatter Radar; Bulk Plasma Drift

15. NUMBER OF PAGES
54

16. PRICE CODE

17. SECURITY CLASSIFICATION OF REPORT	18. SECURITY CLASSIFICATION OF THIS PAGE	19. SECURITY CLASSIFICATION OF ABSTRACT	20. LIMITATION OF ABSTRACT
Unclassified	Unclassified	Unclassifed	SAR

CONTENTS

ILLUSTRATIONS

I INTRODUCTION

The interaction between the solar wind and the earth's geomagnetic field manifests itself in patterns of electric fields in the high-latitude ionosphere. Routine measurement of those fields would be a large step toward an understanding of the detailed coupling between the solar wind and the earth's atmosphere. In fact, determination of high-latitude electric fields has emerged as one of the major outstanding problems in atmospheric science (Kelley, 1990).

The convection of plasma in the polar cap and auroral zones is an effective tracer of the electric field superimposed by the solar wind. Plasma motion can be measured by a variety of methods, using either spaceborne or ground-based instruments. Measurements made directly in the ionosphere are generally unambiguous, but suffer the shortcoming that a one-dimensional measurement in time and space is not adequate to specify the global drift pattern. Only through the use of an unrealistically dense array of satellites and ground stations could the two-dimensional drifts be determined as a function of time. Generally, a system of this type has been judged impractical because of the expense and the task and logistics of data collection and processing. Recently, the potential for such a satellite system has been proposed (Hanson, private communication), but would not be operational within this decade.

Ground-based instruments provide a more practical means for routine observation of high-latitude plasma motion. Four primary categories of instrumentation have been used. These are (1) high-frequency sounding with spaced antennas, (2) high- (or very-high-) frequency coherent-backscatter radar, (3) incoherent-backscatter radar, and (4) spaced-receiver scintillation arrays. Each technique is based on different principles and is sensitive to different indicators of the ionospheric motion; each technique also has its own strengths and shortcomings. We will not specifically discuss the first two of these methods in this report. The effectiveness of the HF ionosonde technique as applied to polar-cap convection has been illustrated by Cannon et al. (1991). HF backscatter radars have been used to measure the motion of small-scale irregularities in the polar cap (Greenwald et al., 1985).

Our interest is with the latter two techniques. The incoherent-scatter radar measures the line-of-sight bulk plasma drift in different directions; from this, a velocity vector can be resolved. The basis of the technique is briefly reviewed in Section II. The transionospheric spaced-receiver scintillation method characterizes the diffraction patterns caused by intermediate-scale irregularities in the ionosphere, which, in the F region, drift with the bulk plasma. The analytical basis of the method and some practical aspects of its application are reviewed in Section III. In Section IV, we compare

simultaneous observations using the two techniques. The data were collected during several periods between 1981 and 1988 at the National Science Foundation (NSF) incoherent-scatter radar operating first at Chatanika, Alaska, and then at Søndre Strømfjord, Greenland. Although the spatial and temporal resolution of the two techniques are very different, under optimum conditions the agreement between the two techniques is good. At other times, the shortcomings of both methods become obvious. From the data sets compared here, we hope to determine the potential of the spaced-receiver technique as a means to make long-term continuous measurements of high-latitude convection.

II INCOHERENT-SCATTER MEASUREMENT OF BULK PLASMA DRIFT

The incoherent-scatter radar (Evans, 1969) is the premier instrument for the study of the large-scale processes in the ionosphere. When the ionosphere is illuminated by the radar signal, electron thermal motion results in scattering. More correctly, the scattering results from variations in the dielectric constant of the plasma corresponding to density changes. The source of these fluctuations are the ions, present in equal numbers with electrons, which cause ion-acoustic waves to be generated when the exciting radar signal wavelength is much longer than the Debye length. Thus, in the data presented here, the ion population dictates the fluctuation spectrum of the backscattered signal; from that spectrum, information can be extracted about both the electrons and ions. In particular, the ion concentration and composition, the electron and ion temperatures and velocities, and ion-neutral collision frequency can be estimated.

In this report, our primary concern is with the bulk motion of the ions and electrons in the upper ionosphere, as driven by large-scale electric fields (e.g., Evans, 1972). The ion-acoustics waves responsible for scatter travel both away from and toward the radar at a speed close to the mean thermal speed of the dominant ions. This produces a damped bimodal spectral form (when collisions are small) with an overall Doppler shift corresponding to drift magnitude. The radar returns, gated in range, are processed to extract this Doppler offset.

The radar is sensitive only to the line-of-sight component of the plasma motion. To obtain a vector velocity, a monostatic radar system must measure the Doppler spectra in different directions. At high latitudes, the plasma motion under normal conditions is primarily horizontal, i.e. the transport parallel to the magnetic field — nearly vertical — is relatively small. Thus, the radar mode geometry should be chosen to provide suitable sensitivity to horizontal plasma motion. The sensitivity of the radar mode is also a function of the received signal-to-noise ratio, which depends on background electron density, the length of the transmitted pulse, and the length of time over which the received signal is integrated.

In practice, various radar modes can be used to obtain resolved plasma drifts. A few of these are discussed in connection with the examples in Section IV. Typical signal-integration times can be between several seconds and minutes to obtain reasonable error statistics from Doppler processing of line-of-sight samples. Geometrically, observations are usually made at elevation angles lower than about 60° to be sensitive to the horizontal drift components. These two factors effectively limit the spatial and temporal resolution of the radar velocity measurements.

Only when the plasma motion is consistent over the time it takes to make the measurements and over the radar field of view will the resolved velocity be accurate. During much of the time, these criteria are satisfied, but they are often violated near high-latitude convection boundaries.

III THE SPACED-RECEIVER TECHNIQUE APPLIED TO TRANSIONOSPHERIC SCINTILLATION DATA

The spaced-receiver radio technique has been used to measure ionospheric motion, with moderate success, for many years. In its simplest form, the concept is that a fading pattern observed from two closely spaced antennas will look similar, but will be delayed in time. Correlation techniques can be used to measure the delay along an antenna baseline pair and, with proper interpretation, the delays measured over multiple baselines provides an estimate of the vector pattern. The use of the technique to estimate ionospheric drifts with using an ionosonde was first suggested by Mitra (1949). There have been improvements of that original concept, allowing for diffraction pattern rearragnement with time, and recognition that anisotropic contours of correlation would affect velocity measurements. Briggs et al. (1968) reviews the range of these technique modifications.

The technique is readily applied to interplanetary scintillation and transionospheric satellite observations. In this case, the signal source is a radio star or a transmitter aboard a satellite and a scintillation fading pattern is observed at a ground station using an array of antennas. In the transionospheric case, the pattern being analyzed is the integrated result of scattering by electron density irregularities along the radio raypath through the ionosphere. It is then necessary to identify the relationship between the *in situ* irregularity structure and drift with the corresponding characteristics of the diffraction pattern. For UHF radio frequencies applied to transionospheric paths, it is appropriate to make this association using thin phase-screen theory. The analytical details of the thin phase-screen theory can be found in a number of papers, notably Rino (1979). For our purposes, it will suffice to summarize the applicability of the assumptions made in the theory and its conclusions regarding spatial correlation forms.

The tacit assumption in the thin-phase-screen theory is implied by its name: the intensity and phase of the radio wavefront emerging from a layer of irregularities can be reproduced by a thin, phase-changing screen in the ionosphere. In the high-latitude ionospheric case and a UHF probing frequency, the assumption appears to be robust. In the equatorial case, which is often more difficult to justify, it has been shown that the thin-phase-screen interpretation of phase-spectral forms is fully consistent with irregularity spectral forms measured *in situ* (Livingston and Dabbs, 1986).

Generally speaking, the *in situ* irregularities can be characterized as having a three-dimensional spatial autocorrelation function. For a radio raypath propagating through a layer of these irregularities, the thin-phase-screen theory predicts a corresponding two-dimensional form of the scintillation fading pattern. For example, if the

irregularities have a spheroidal correlation form, the diffraction pattern will have elliptical contours of correlation. Rino (1982) shows that, in the weak-scatter scintillation case, the fading pattern correlation surfaces are the same for the intensity and phase of the received scintillation signal. Because of Fresnel filter effects, the spatial decorrelations lengths are quite different, but the forms are the same. In the strong-scatter scintillation case, the same correlation surface form continues to hold as the disturbance level increases, even into saturation.

The characteristics of the correlation surface of a scintillating signal can be measured from an array of antennas on the ground, and information can be extracted from those data using a variety of techniques (Briggs, 1968). The method applied to the data in Section IV is an adaptation of that of Armstrong and Coles (1972), for which the only restriction on the shape of the autocorrelation surface is that it be quadratic. The technique uses the intersections between the various auto- and cross-correlation functions of the time series at three or more antennas.

An important concept in the spaced-receiver technique is that the correlation surface is affected by both the anisotropy of the pattern and its drift. Armstrong and Coles (1972) applied their technique to interplanetary scintillation, assuming an isotropic irregularity form, to obtain solar wind drift estimates. However, they pointed out that if the cross-correlation peaks could be accurately measured, the pattern drift and the anisotropy could be determined simultaneously. This extension of the method is addressed by Rino and Livingston (1982).

At VHF and UHF frequencies, the ionospheric irregularities that produce the scintillation have a cross-field spatial dimension between a few hundred and a few thousand meters. The irregularities are only rarely isotropic, because of the high electrical conductivity along the local magnetic field direction. The two-dimensional signal correlation surface observed on the ground will reflect the irregularity anisotropy, and will be additionally altered by geometrical projection. It becomes critical to extract this anisotropy accurately to obtain the drifts. A simple example of why this is true is a case where the major axis of the correlation ellipse lies along a spaced-receiver baseline. The high degree of correlation between that antenna pair would imply an extreme velocity along the baseline if one simply divided the distance by the delay parameter. This would be true even if the irregularities producing the pattern were stationary. In general, there is a significant difference between apparent and true pattern velocities. This is particularly true when the signal source is an orbiting satellite and the propagation geometry changes rapidly with time, as has been shown by Rino and Livingston (1982).

In practice, a number of conditions and situations can limit the application of the spaced-receiver scintillation technique to the measurement of ionospheric drifts. Some of these limitations are placed by ionospheric conditions. A primary requisite is that there be adequate irregularity structure to measurable signal fluctuation at the system

operating frequency. This is generally not a problem at high latitudes, where long-term observations show that some irregularity structure is normally present. The path-integrated nature of scintillation is also a potential problem. If the irregularities with different characteristics at different altitudes contribute to the fading, the methods will not properly extract either anisotropy or drift. Fortunately, the irregularities that most affect the propagation are near the peak of the F layer, simply because of higher background density. Thus, there is generally a minimum of ambiguity resulting from integration through layers of different anisotropy and drift.

Geometrical factors also play a role in the spaced-receiver analysis. A high elevation angle to the signal source is ideal for many reasons. It minimizes the integration effects by shortening the raypath length through the ionosphere and also minimizes the geometrical exaggeration of the pattern anisotropy. Numerically, it becomes increasingly more difficult to obtain pattern drift information as the pattern anisotropy increases. At some point, the spaced-receiver baseline becomes too short to observe adequate spatial decorrelation of the pattern (Costa and Fougere, 1988). Basu et al. (1991) have demonstrated that it is difficult to determine the drift velocity of the irregularities associated with patches within the central polar cap owing to the high anisotropy of these irregularities. On the other hand, they have shown that drift reversals associated with arcs can be determined in view of the moderate values of anisotropy of arc-associated irregularities.

These practical aspects of the scintillation technique are further discussed in the examples that follow.

IV DATA COMPARISONS

There have been several periods during which a three-antenna spaced-receiver system has been operated in conjunction with the NSF incoherent-scatter radar. The first of these were campaigns at Chatanika, Alaska, in 1981-1982, and then from 1983 to the present after relocation of the system to Søndre Strømfjord, Greenland. Unfortunately, directly comparable data sets between the two instruments are rare.

We here discuss five data sets. The first two of these were from early campaigns, one from Chatanika and the second from Søndre Strømfjord; these compare the spaced-receiver-derived drifts with those measured during routine radar operating modes. The second series of examples are from a March 1988 campaign at Søndre Strømfjord dedicated to radar/scintillation drift comparisons. A specialized radar mode was used for these observations to allow detailed comparisons between the two instruments. These illustrate the strengths and shortcomings of both the radar and spaced-receiver techniques. They also suggest some specialized application of the spaced-receiver technique to observe small-scale velocity structure.

A. Chatanika, Alaska, 11 November 1981

Prior to the move of the NSF radar from Chatanika, Alaska to Søndre Strømfjord, Greenland, a scintillation system was installed at Poker Flat and operated during campaign periods. The first of these campaigns was in November 1981, when the radar was collecting synoptic data during DE-1 and TRIAD satellite overpasses. The radar mode for these experiments consisted of two approximately north-south scans: an elevation scan in the magnetic meridian, followed by a composite azimuth/elevation scan to the west. The geometry of the scans was such that the local solar time of the scans was similar; that is, the data from the northmost point of the composite scan corresponded, in solar time, to the data taken during the meridian scan some 10 minutes before. If it is assumed that the ionospheric conditions are "frozen" over the local time and latitude extent of the scans, pairs of line-of-sight velocities from both scans can be used to resolve the vector plasma drift as a function of latitude.

Figure 1 shows the geometry of the radar mode on 11 November 1981, as operated in conjunction with a DE-B satellite overpass. Shown on the map are the radar scan locations in latitude and longitude at the altitude of the DE satellite (approximately 350 km). The ionospheric penetration point of the spaced-receiver scintillation raypath

(elevation angle 57° at an azimuth of 280°) falls between the centers of the two radar scans. Figure 1 also shows the DE-B subsatellite track.

Figure 2 shows the radar-measured vector velocities at an altitude of 350 km in a clock-dial format. The gap in the resolved velocities near overhead is simply because, at that geometry, the radar line-of-sight velocity pairs are insensitive to any horizontal, magnetic north-south component of motion. The period of interest for this evening is between 0400 UT and 0800 UT, which is the time that the propagation geometry of the scintillation experiment remained constant. The time of the DE-B overpass at the radar latitude was about 0540 UT. As can be seen, the plasma drift was consistently westward during the experiment at a maximum speed of about 700 m/s. From the plot, it can be seen that there is a some latitudinal variation in the drift magnitude, and slight changes in the drift direction between 0400 UT and 0800 UT.

Figure 3 shows a series of electron density profiles at the latitude of the radar measured at various times during the experiment. The F-region peak electron density was high, close to 10^6 cm^{-3}, at an altitude of 350 km. During this part of the evening, there was no enhanced hard particle precipitation; the E-layer peak densities are at a typical diffuse auroral level near 10^5. In terms of the scintillation signal, the altitude and density of the F-region peak suggests a single layer of dominating irregularities. This, and the relatively consistent and simple pattern of radar-measured drifts, implies a straightforward data set for comparison of the radar and scintillation techniques.

As discussed in Section III, the spaced-receiver extraction of drift information requires simultaneous and accurate extraction of the anisotropy and orientation of the measured scintillation correlation surface at the receivers. Figure 4 shows the axial ratio and orientation of the measured scintillation correlation surface. The measurements are shown with respect to two *in situ* irregularity types at an altitude of 350 km with 10:1 and 20:1 field-aligned extensions. Both irregularity shapes produce an orientation of the correlation pattern, that is very consistent with the measured pattern. The orientation agreement confirms that the irregularities are concentrated near the F-region peak altitude. The axial ratio of the measured pattern suggests that there is some variation in the anisotropy of the in situ structure, but it is well bracketed between about 10:1 and 30:1. These are typical of anisotropies observed in the evening auroral zone (Livingston et al., 1982). As a practical matter, the relatively small pattern anisotropies (less than about 8:1) and the excellent agreement between the measured and predicted orientation suggest that the simultaneously extracted pattern velocity data should be of high quality.

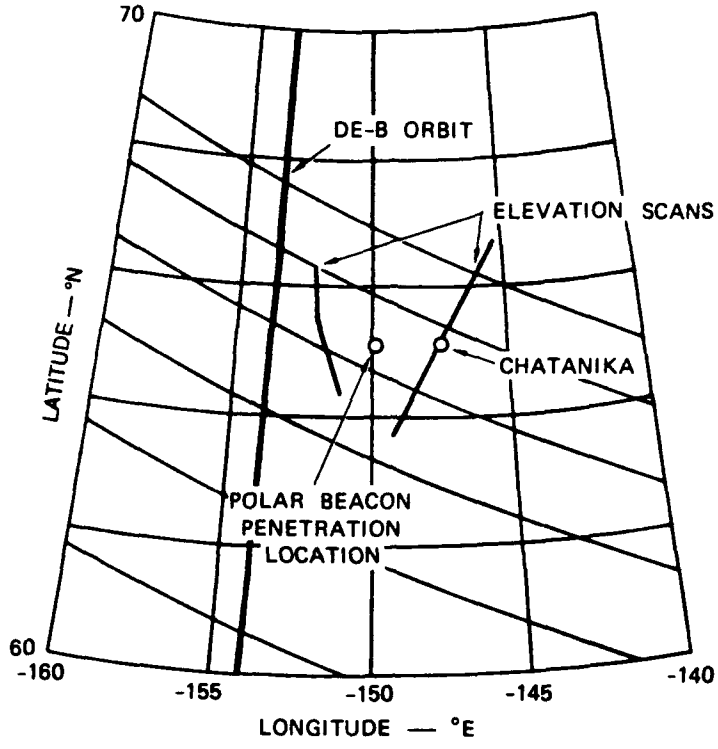

FIGURE 1 EXPERIMENT GEOMETRY ON 11 NOVEMBER 1981, SHOWING RADAR SCANS, PROPAGATION INTERCEPT, AND DE-B SATELLITE GROUND TRACE

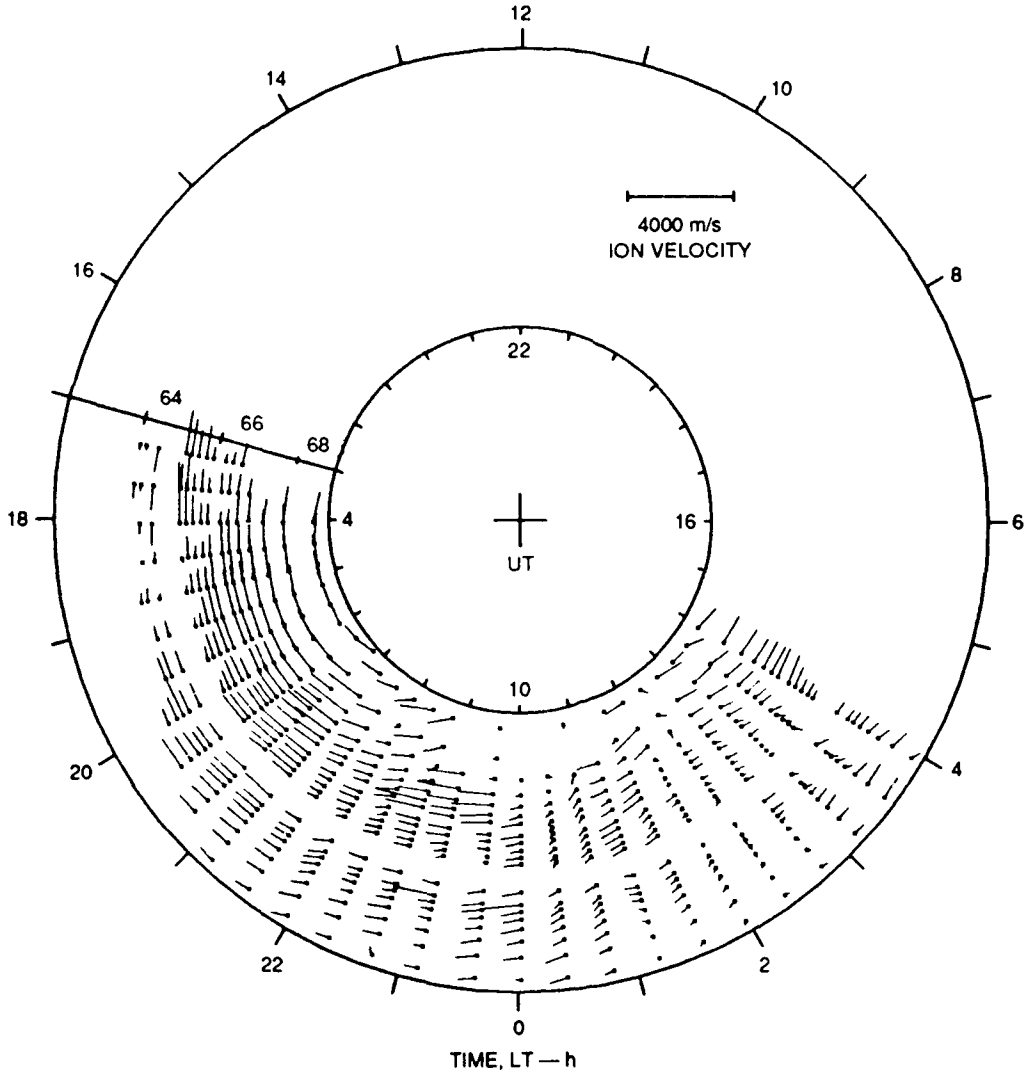

FIGURE 2 RADAR MEASURED PLASMA DRIFT DURING 11 NOVEMBER 1981 EXPERIMENT

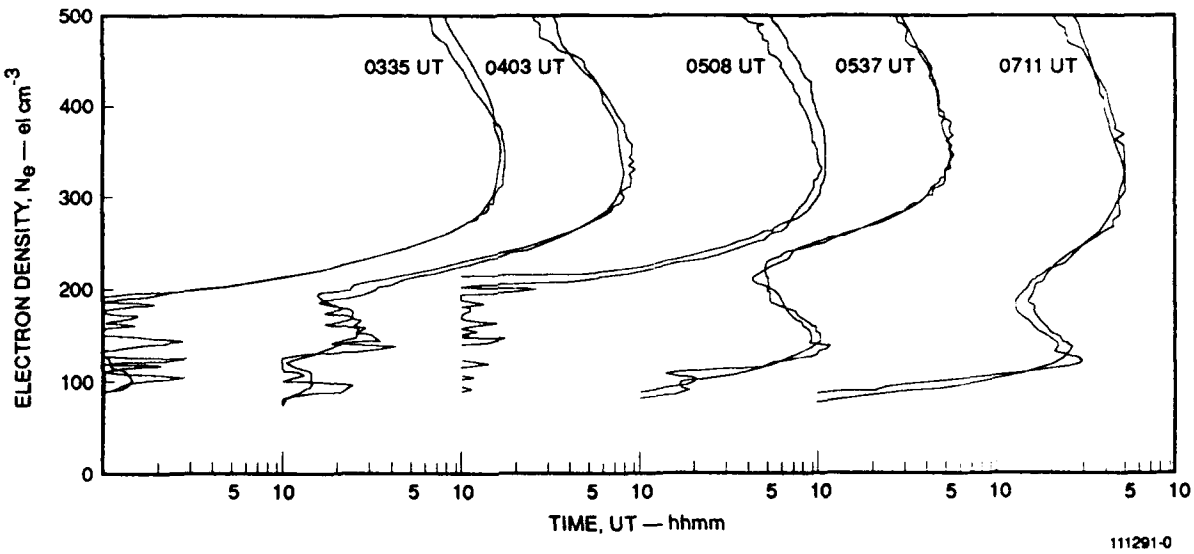

FIGURE 3 ELECTRON-DENSITY PROFILES DURING 11 NOVEMBER 1981 EXPERIMENT

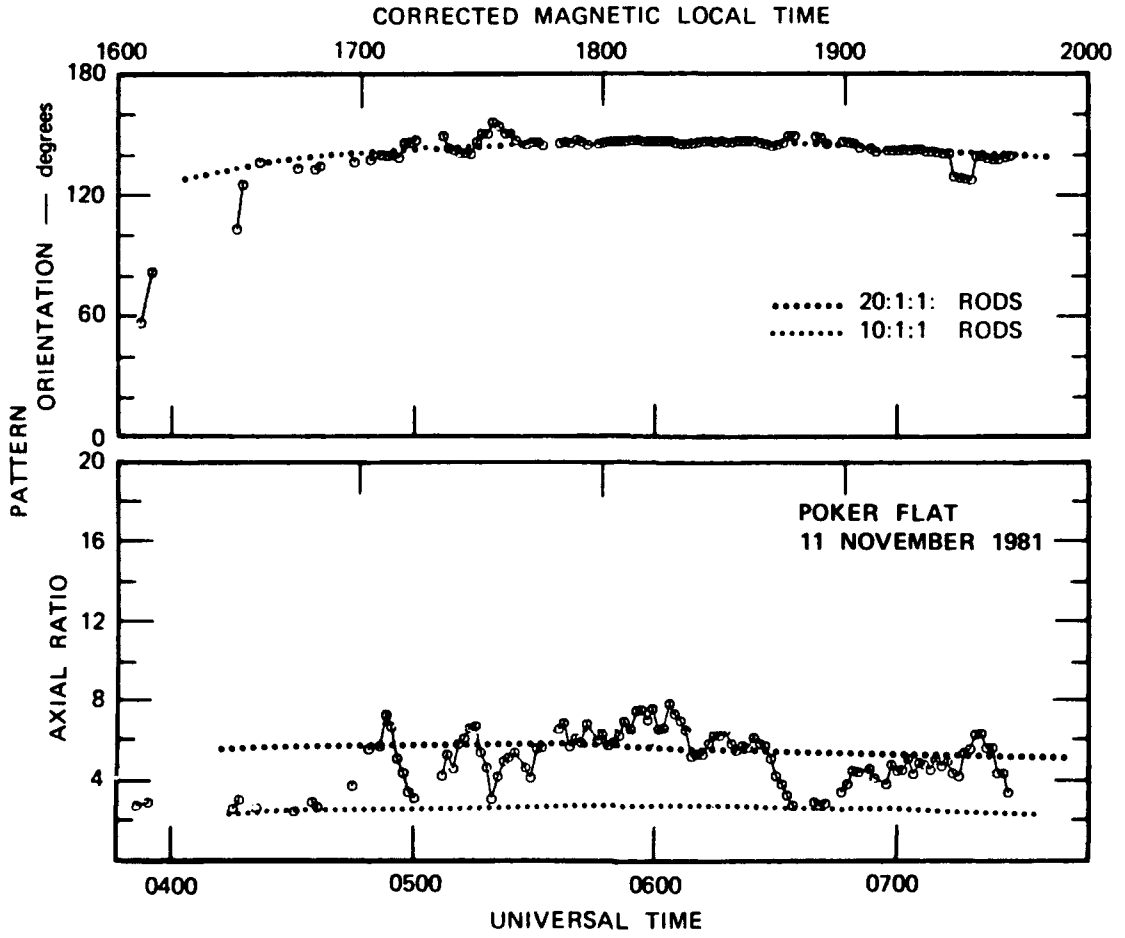

FIGURE 4 OBSERVED SCINTILLATION CORRELATION SURFACE PARAMETERS DURING 11 NOVEMBER 1981 EXPERIMENT

The spaced-receiver-measured irregularity drift is shown as a function of time in Figure 5. In this case (and the others in this report) the scintillation data are processed in overlapping 80-s blocks, producing a velocity estimate every 40 s. Also shown are the radar-measured plasma drifts at approximately the same latitude as the scintillation penetration point. The basic cycle time of the resolved radar drifts is about 20 min, as the points in the figure show. Because there was a break in the routine scans to track the DE-B overpass, there is no resolved velocity estimate between 0505 UT and about 0550 UT. As can be implied from the component velocities, there is good agreement between the drift magnitudes in Figure 5, but some discrepancy in drift direction up until about 0600 UT. Also superimposed is the cross-track velocity component measured by DE-B at the same invariant latitude as the scintillation penetration point, but at a longitude considerably to the west. Unfortunately, there was no north-south (RAM component) velocity measurement available from DE-B. The spaced-receiver drifts correspond exactly to the DE-B observations, although the agreement may be to some extent, fortuitous.

We argue that the difference between the radar and the scintillation techniques in Figure 5 is a result of the spatial/temporal smearing inherent in the radar mode used. That mode is a compromise between latitudinal coverage and temporal/spatial resolution. At an altitude of 350 km, the longitudinal separation of the meridian and composite scans is more than 200 km, and the line-of-sight velocity pairs are measured 10 min apart in real time. The assumption that the auroral motion is frozen in invariant latitude and solar time is good only to first order. Furthermore, the sensitivity of the radar to north-south components of velocity is poor at the latitudes near the radar. If there are small but conflicting north-south components in the line-of-sight velocities, the difference in direction which we see in Figure 5 could easily arise. The spaced-receiver irregularity drift is likely to be a more accurate indicator of the plasma motion at the latitude and longitude of the penetration point than the resolved radar plasma drift.

B. Søndre Strømfjord, Greenland, 13 April 1983

The NSF incoherent scatter radar was relocated to Søndre Strømfjord, Greenland during 1982, and resumed operation in early 1983. In March 1983, the spaced-receiver system from Poker Flat was installed at the radar facility and was operated daily for a number of weeks. The first extended, collaborative radar/spaced receiver velocity comparisons are from the World Day observations on 13-14 April 1983.

The radar mode for this particular World Day consisted of 11 fixed-position dwells and a 5 min elevation scan through the magnetic meridian. The line-of-sight velocity measurements from the 11 dwells are taken in various combinations to resolve vector velocities as a function of latitude and time. The cycle time of the mode is approximately 20 min. As with the previous example, spatial and temporal resolution of the resolved

velocity must be traded off against spatial coverage, which is extensive in this case (approximately 1100 km in the F layer).

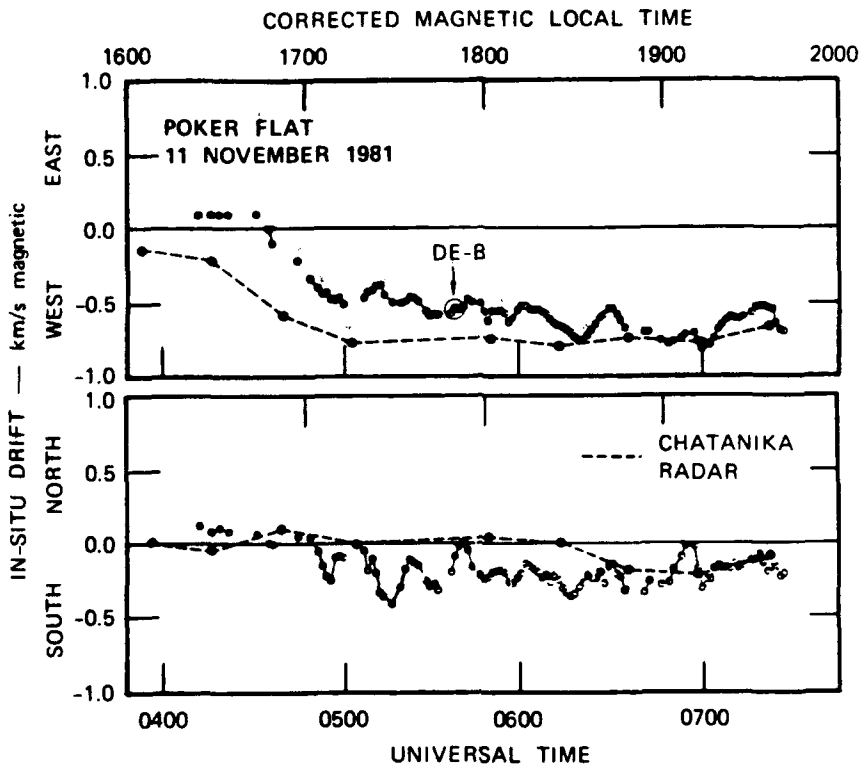

FIGURE 5 COMPARISON OF VELOCITY COMPONENTS MEASURED BY SPACED-RECEIVER (DOTS) AND RADAR (DASHED LINE)

The overall drift pattern for the entire 24-hour run is shown in a clock dial format in Figure 6. The complexity of the ionospheric dynamics (which is typical at Søndre Strømfjord because of its proximity to the auroral/polar convection reversal boundary) is clear during several portions of the run. Our interest here is with the block of time between 1730 UT and 2130 UT when the scintillation radio source was at a nearly constant position overhead of the radar. Between 1730 UT and about 1945 UT, the data show that the convection reversal boundary was directly overhead of the radar, at an invariant latitude of about 74°. After that time, the boundary moved southward until it was out of the radar field of view by about 2100 UT.

For this period of time, the ionospheric F region passed from sunlit to dark conditions, although the electron density distribution in latitude was simultaneously being altered by convection. Representative profiles of electron density during this time period are shown in Figure 7. The solar-produced electron density near 1800 UT peaks at about 4.5×10^5 at an altitude of about 280 km. As the overhead region passes into darkness, the electron density decreases to less than 2×10^5 and the layer broadens and rises to about 350 km. After 2100 UT, the F-region scale height becomes very large. If there are significant differences in the density structure or its motion with altitude (e.g., a velocity shear in altitude), integrating through such a layer would distort the spaced-receiver data.

Figure 8 shows the radar data for the time period of interest in an invariant latitude vs. time format. As with the 11 November 1981 data, the radar cannot, in this mode, obtain enough of a line-of-sight velocity component near overhead to resolve the horizontal velocities. The transition of the convection boundary from near overhead early in the period to about 70° invariant by 2100 UT is clear in the figure, however. Figure 8 also shows the vector velocities measured by the spaced-receiver technique. There is a slight change in the satellite position (and thus the raypath penetration point latitude) over the viewing period. As with the 11 November 1981 data, there is a velocity estimate every 40 s; a 10-point smoothing has been applied to the data in the figure.

It is difficult to quantitatively compare velocity magnitudes in the format of Figure 8, but the agreement between the spaced-receiver and radar plasma drift is generally good. Early and late in the experiment, the velocity magnitudes appear to disagree, although the difference is within the error bars of the radar measurement. During the slow but systematic transit of the velocity-reversal boundary, the velocity directions and magnitudes agree well. The high time resolution of the spaced-receiver data provides some insight into the velocity structure that accompanies the convection reversal boundary, which is below the spatial resolution of this particular radar mode.

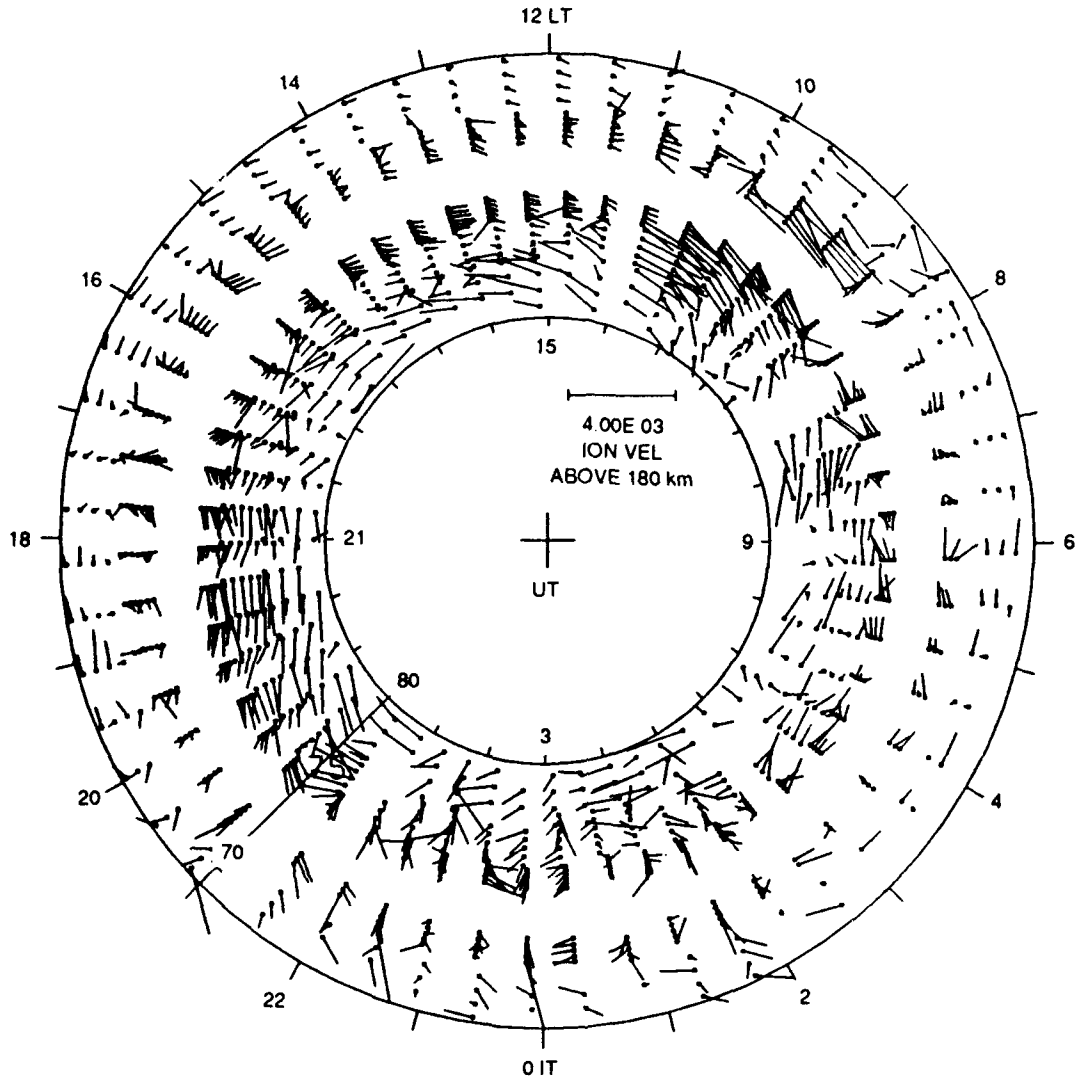

FIGURE 6 RADAR-MEASURED PLASMA DRIFT DURING 13 APRIL 1983 EXPERIMENT

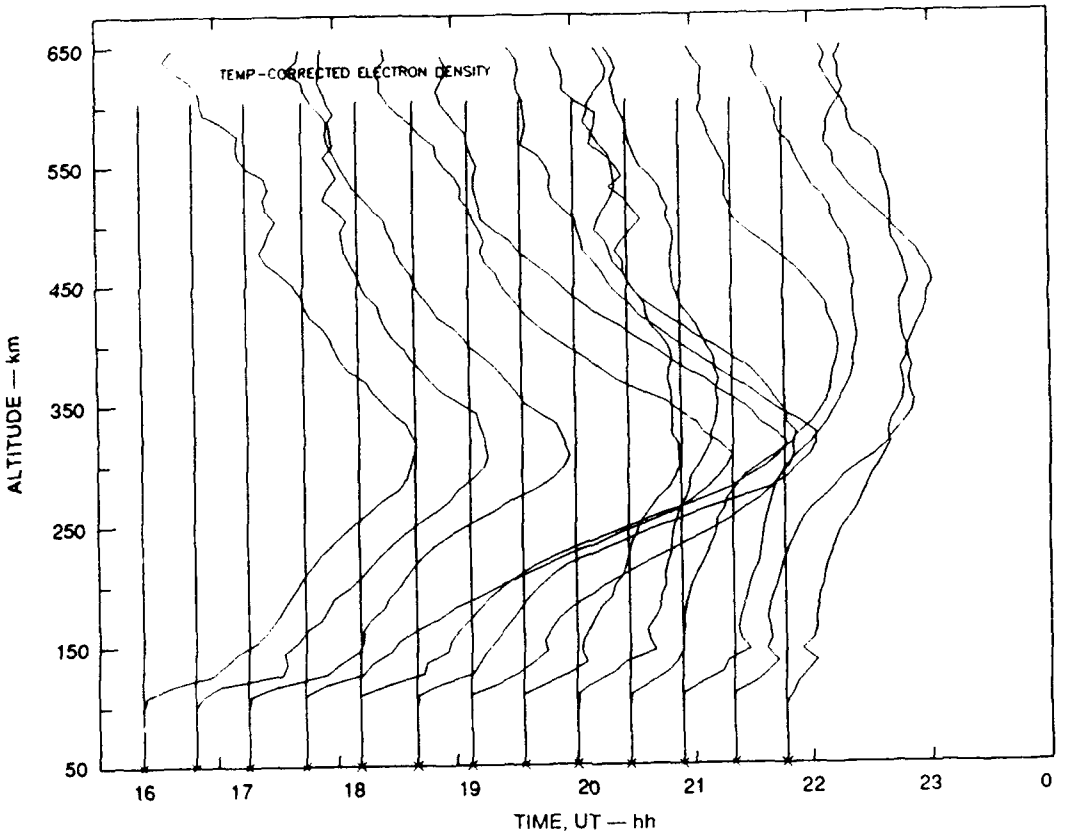

FIGURE 7 ELECTRON-DENSITY CONTOURS DURING DURING THE 13 APRIL 1983 EXPERIMENT

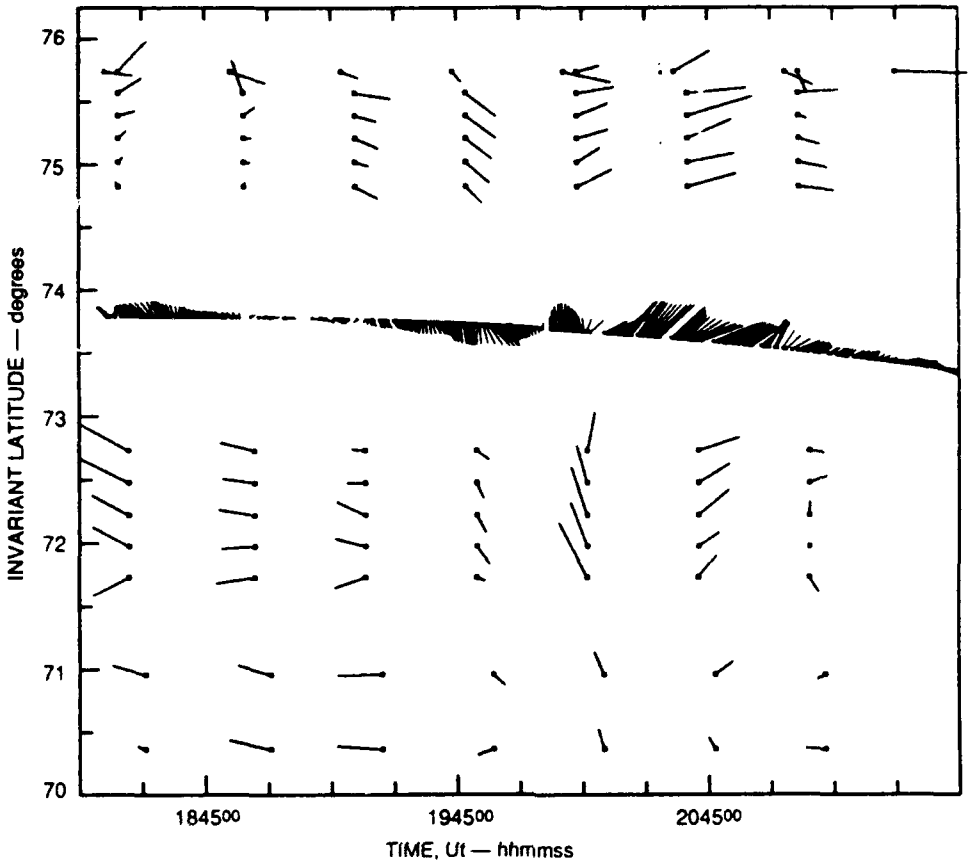

FIGURE 8 COMPARISON OF IRREGULARITY VELOCITY MEASURED BY SPACED-RECEIVER AND LARGE-SCALE DRIFTS MEASURED BY RADAR DURING 13 APRIL 1983 EXPERIMENT

C. Søndre Strømfjord, Greenland, 22 March 1988.

In late March 1988, a series of Sondrestrom radar runs were dedicated to coincident spaced-receiver drift measurements. Observations were made on 21-23 March during the local afternoon hours, and during the early morning on 25 March. Each period corresponded to times when one of the satellite signal beacons was near Atlantic apogee. As discussed above, the high elevation angle geometry (about 73° to the east in this case) reduces the complexity of interpretation of the spaced-receiver-derived parameters.

A radar mode was designed to minimize the spatial and temporal smearing inherent in the method. It consisted of a vertical dwell plus four fixed positions centered on the scintillation propagation direction followed by a rapid, circular azimuth scan. The dwells, each of which was 20 to 45 s long, provide electron-density profiles and the traditional multiposition resolved velocity. However, the angular separation of the positions was minimized to reduce the local time/latitude smearing of the resolved velocities. The circular azimuth scan was made over 300 s, at an elevation angle of 60°. The scan was chosen to provide a quick look at the velocity structure in the vicinity of the radar and scintillation penetration points. The line-of-sight velocities from such scans are very useful, by themselves, as they provide a means to identify rapidly evolving shear regions. Furthermore, when combined over some limited angular sector, those velocities can be resolved into directional components. This can provide — with certain limitations — higher time resolution bulk motion velocity patterns than the fixed dwells. The total cycle time for the fixed positions and scan was about 7 min. This is considerably shorter than the routine radar experiment cycle times, such as the World Day mode used for the 13 April 1984 data.

On 22 March 1988, observations were made between about 2000 UT and 0000 UT. Within this window were two nearby passes of the HILAT satellite, at 2115 UT and 2256 UT, which had a particle detector and drift meter aboard. Data from these instruments show that the convection boundary was indistinct during this evening, and a generally chaotic velocity pattern was seen by the satellite. However, the radar was just at the northern edge of a hard particle precipitation boundary, so the likelihood of latitudinal and local time velocity structure is high.

Figure 9 shows a pattern of velocities measured by the radar, resolved from the azimuth scans. These correspond to an altitude of approximately 270 km (near the F-region peak). These data were derived from 10-s integrations of data during the 300-s continuous scans; this provides 30 line-of-sight velocity samples around the circle. Each set of six consecutive samples (an 84° sector) is then used to resolve a running series of velocities. Of course, the eastern and western points in the azimuth scans cover a significant range of local time. To represent the data in terms of a spatial pattern of drifts, the western azimuth vectors are plotted in Figure 9 according to the time offset equivalent to their longitude separation from the radar.

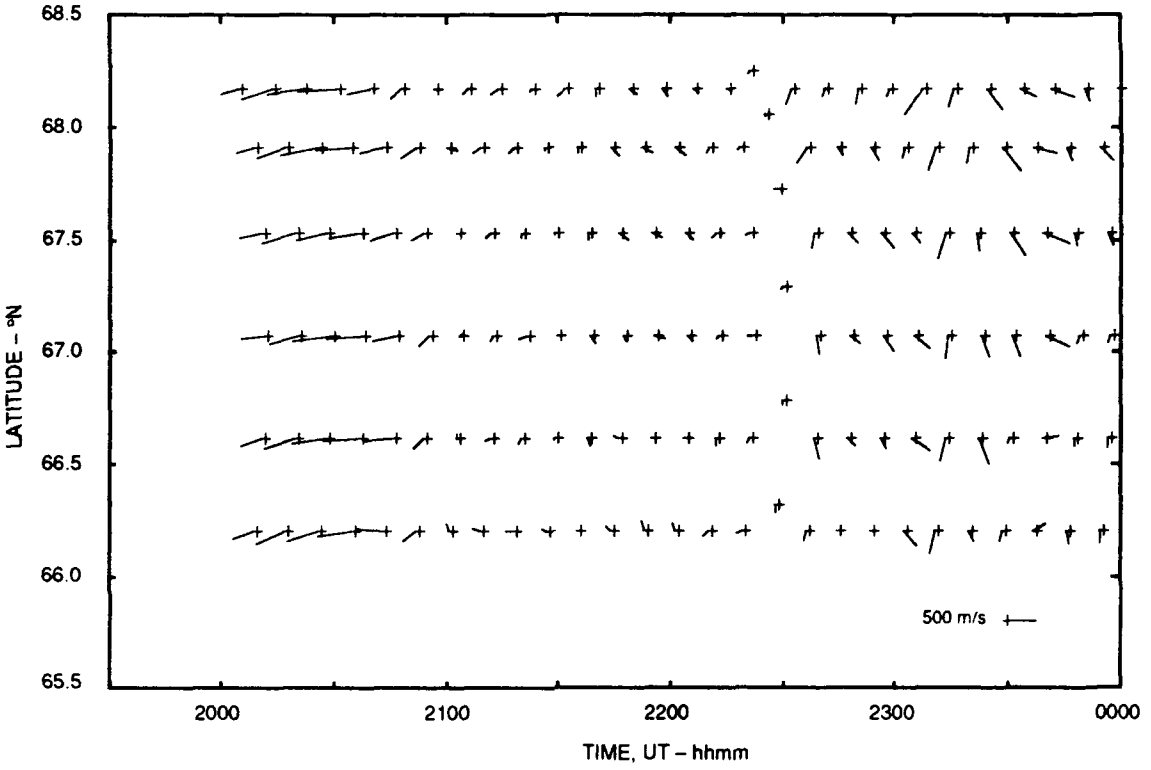

FIGURE 9 PATTERN OF VELOCITY AT AN ALTITUDE OF 270 km RESOLVED FROM RADAR SCAN DATA DURING 22 MARCH 1988 EXPERIMENT

The purpose of the figure is to characterize the degree of complexity of the local ionospheric dynamics during the 4-hour experiment period and to identify the specific times and locations of convection boundaries, should they pass through the field of view.

A more traditional set of vector velocities is resolved from the four fixed position dwells. The four positions are: vertical, satellite raypath direction (azimuth 90°, elevation 73°), 65° elevation in the magnetic west direction, and approximately up the magnetic field. The spatial resolution of that resolved vector velocity is more typical of routine radar operations than the rapid azimuth scans. These velocities are plotted in Figure 10 as function of altitude and time from the lowest altitude long-pulse gate at 120 km through the topside of the F region.

The data from Figure 10 can be roughly construed as a vertical cut through the center of Figure 9 at an altitude of about 270 km. Comparing Figures 9 and 10 in this way, the overall large-scale plasma features correspond reasonably well, but there are differences — particularly near 2200 UT and 2300 UT — when the convection boundary appears to pass overhead. We will be making note of several of these periods when the comparisons are made with the spaced-receiver irregularity drift data. The differences are not surprising, judging from the complexity of the scan-resolved drift patterns in time and space, plus the different spatial resolution of the two modes.

Also of interest are the magnitude and altitude of the electron density during the observations. These directly affect the integrated scintillation measurements, but can also be indicators of whether the polar cap, the auroral zone, or both are within view of the radar. Figure 11 is a sequence of electron-density profiles, as derived from the vertical dwell position. There are several points to be made from the figure. First, there is negligible E-region electron density throughout the evening, relative to the F-region peak. Secondly, from the beginning of the experiment through about 2030 UT, the F layer has a peak density of about 2×10^5 and is relatively broad in altitude. We might accordingly suspect some altitude smearing in the integrated scintillation data. As the peak F-layer electron density increases with time, the bottomside density decreases and the layer width narrows.

The "background" scintillation data for this experiment are shown in Figure 12. The bottom two frames are the measured pattern axial ratio and orientation of the measured correlation surface. As noted above, these parameters provide a first-order check on the diffraction pattern extraction, which must be accurate for the velocities to be valid. The top frame in Figure 12 is the S4 Briggs and Parkin (1963) intensity-scintillation index, computed as the normalized standard deviation of signal intensity. The index saturates at about 1.2, corresponding to very strong scatter. As mentioned above, theory predicts that diffraction effects in strong scatter do not upset the correlation surface shape; however, diffraction does affect the decorrelation times of the intensity signal.

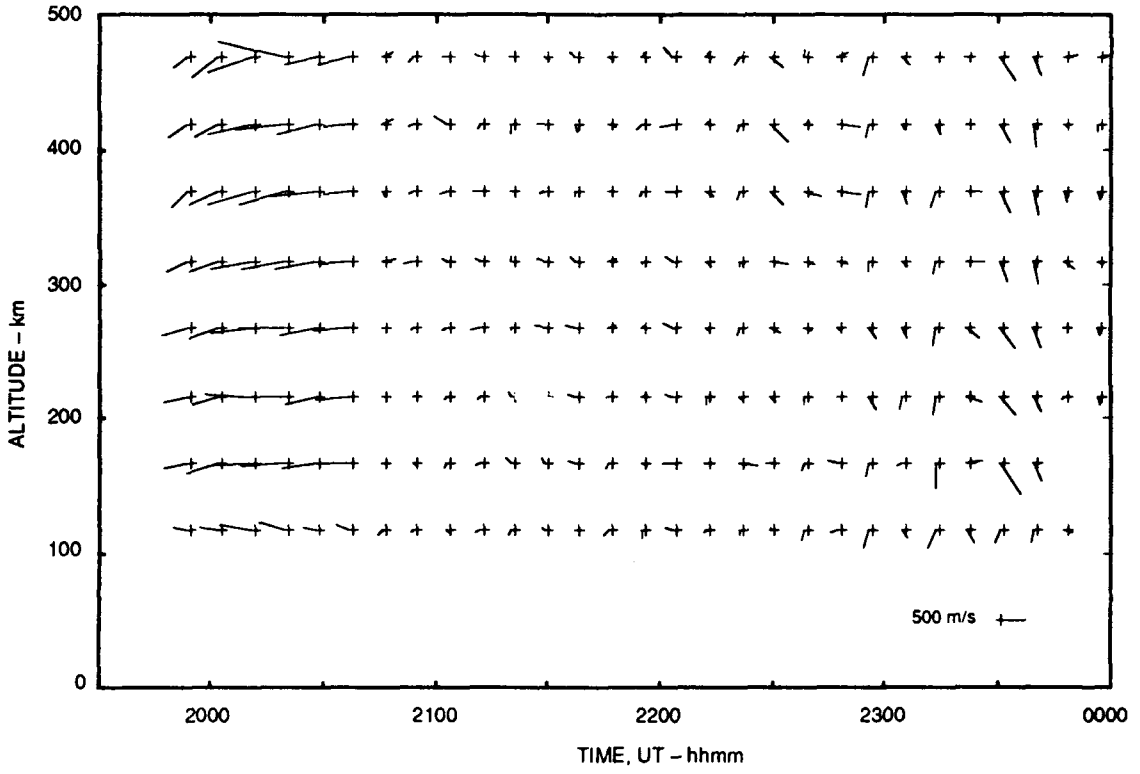

FIGURE 10 ALTITUDE PATTERN OF VELOCITY RESOLVED FROM RADAR MULTIPOSITION DWELLS DURING 22 MARCH 1988 EXPERIMENT

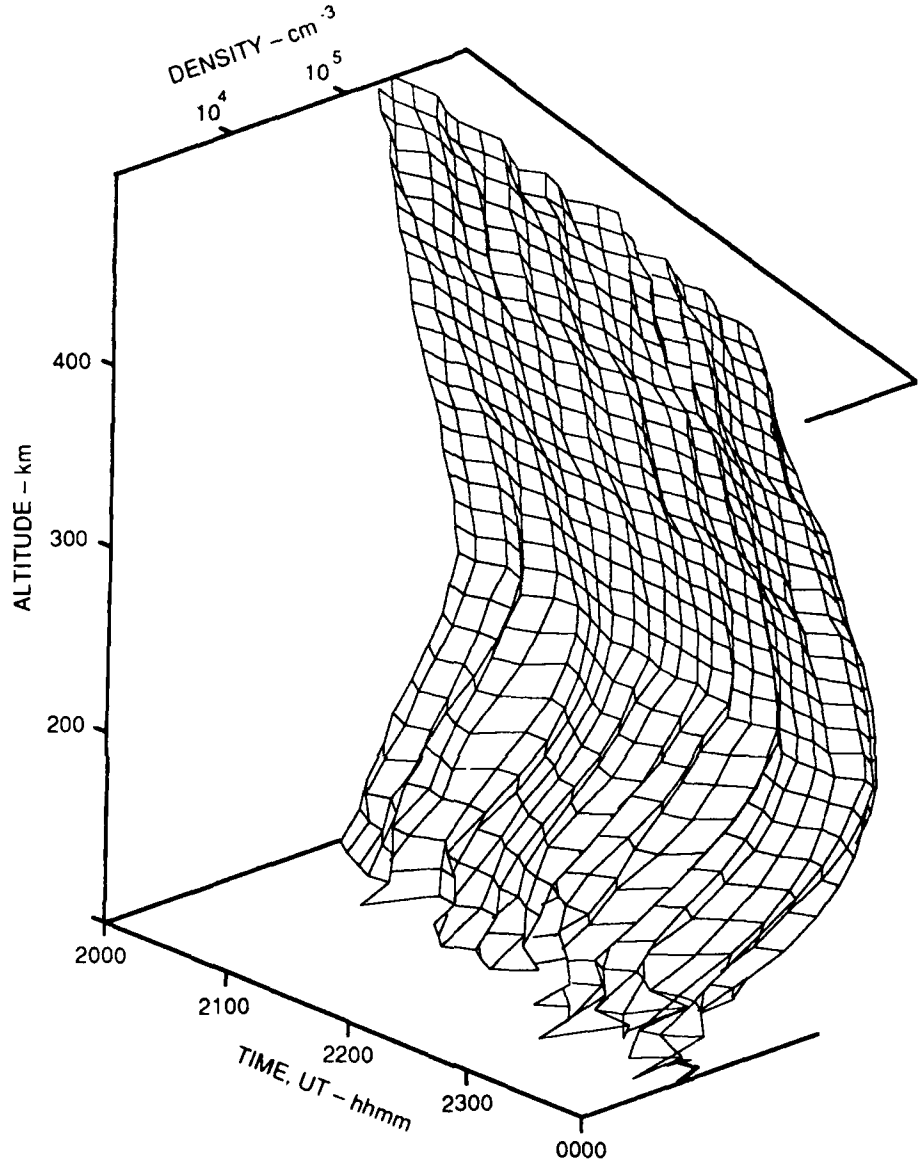

FIGURE 11 ELECTRON DENSITY PROFILES DURING 22 MARCH 1988 EXPERIMENT

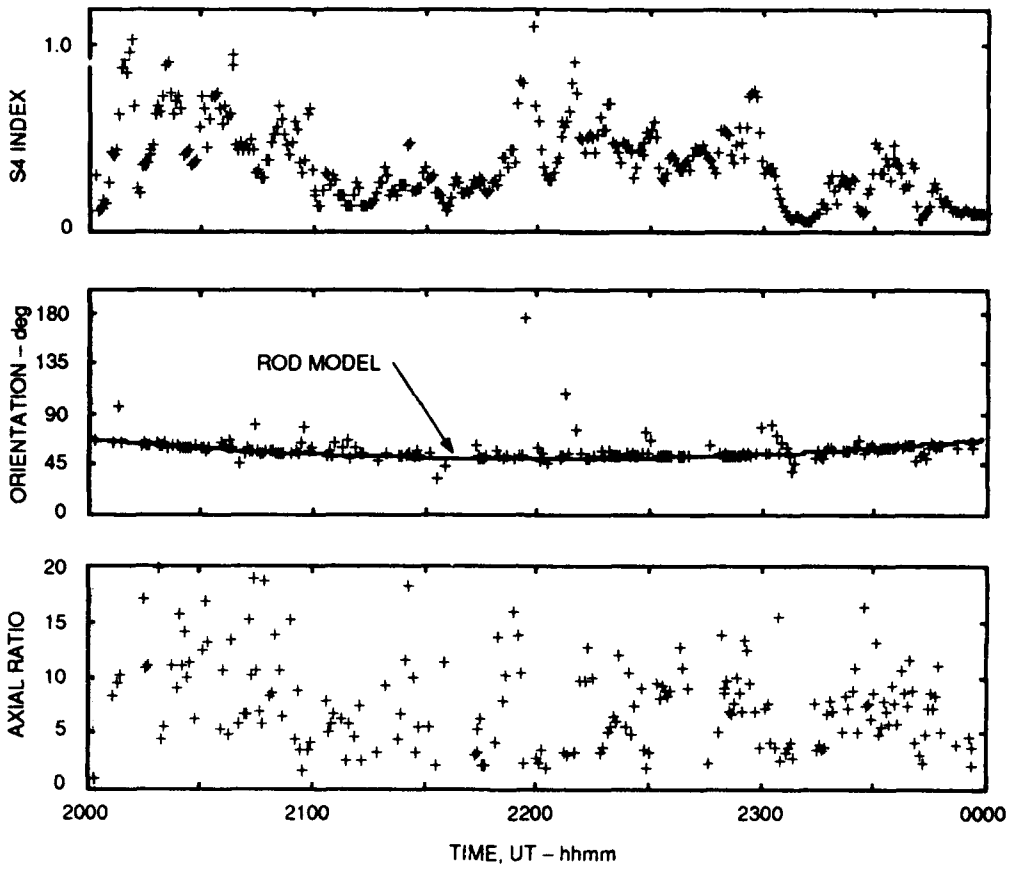

FIGURE 12 OBSERVED SCINTILLATION INDEX AND CORRELATION SURFACE PARAMETERS DURING 22 MARCH 1988 EXPERIMENT

The S4 plot shows that three or four intensely structured patches of irregularities pass through the scintillation raypath early in the window, despite the relatively low background electron density. At these local times, these are probably bunches of ionization which have been convectively structured throughout their passage across, and exit from, the polar cap.

Figure 13 shows the spaced-receiver irregularity drift estimates in terms of magnitude, direction, and geographic components. In the figure, individually derived spaced-receiver velocity values are marked as plus signs. In addition, a running fit has been applied (as derived from a 10-point binomial smoothing algorithm) to identify trends in the data, if any. We have observed that very strong intensity scatter (S4 > 0.7) often produces inconsistent results from record to record, and those points have been removed from these data. Under weak scatter conditions, the correlation computations can also be inconsistent, but have been retained in the figure. There are some general features to note about Figure 13. The north-south velocity component appears to be much less noisy than the east-west component. This is partially a function of the spaced-receiver baseline orientation relative to the major axis of the pattern correlation ellipse. (This sensitivity of the derived parameters as a function of baseline orientation would be alleviated by addition of a fourth spaced-receiver.) The scatter in the east-west velocities might also be real, because the ionosphere at these latitudes is prone to shears in time (Tsunoda, 1988). There is support for this concept in that there is also generally better agreement between the spaced-receiver data and the radar-measured north-south velocity components (as will be shown in the figures that follow). Whatever the source of the east-west velocity spread, the general trend in the drift magnitude and velocity can be tracked.

The data from Figure 13 are overplotted in Figure 14 with radar data from Figures 9 and 10. This format enables direct quantitative comparisons between the two techniques. The heavy dark lines are the resolved velocities from the 270-km altitude gate of the vertical dwell; the heavy dashed line shows the resolved velocity from the azimuth scans in the direction most closely aligned with the scintillation raypath. The overall agreement between all three is relatively good, although there are periods in the data where the three observations are clearly different, and even contradictory. We will compare these in more detail to see how they relate to the radar and spaced-receiver techniques under these ionospheric conditions. Unfortunately, the radar data were not analyzed in a way that allows assignment of rigorous error bars, which would be very useful in the comparisons we will make. Similarly, there are no error bars on the spaced-receiver data.

There is a discrepancy between the radar-derived dwell and scan velocities at the beginning of the observation window (2000 to 2030 UT). Looking at the component line-of-sight velocities used to derive these quantities suggests that, despite a large and dominant westward drift, there is considerable spatial variation in the observed Doppler shifts.

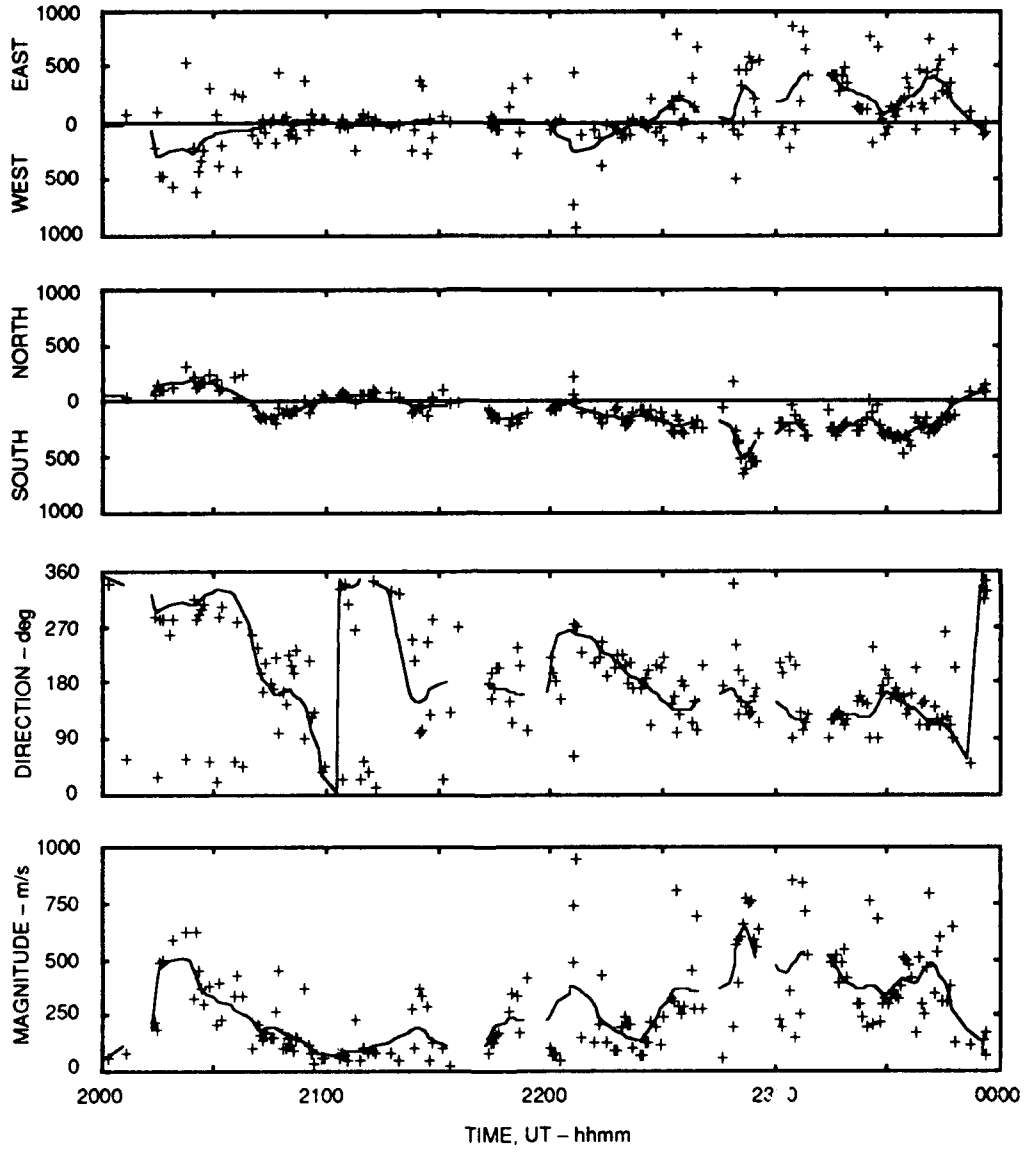

FIGURE 13 IRREGULARITY VELOCITY MEASURED BY SPACED-RECEIVER DURING 22 MARCH 1988 EXPERIMENT

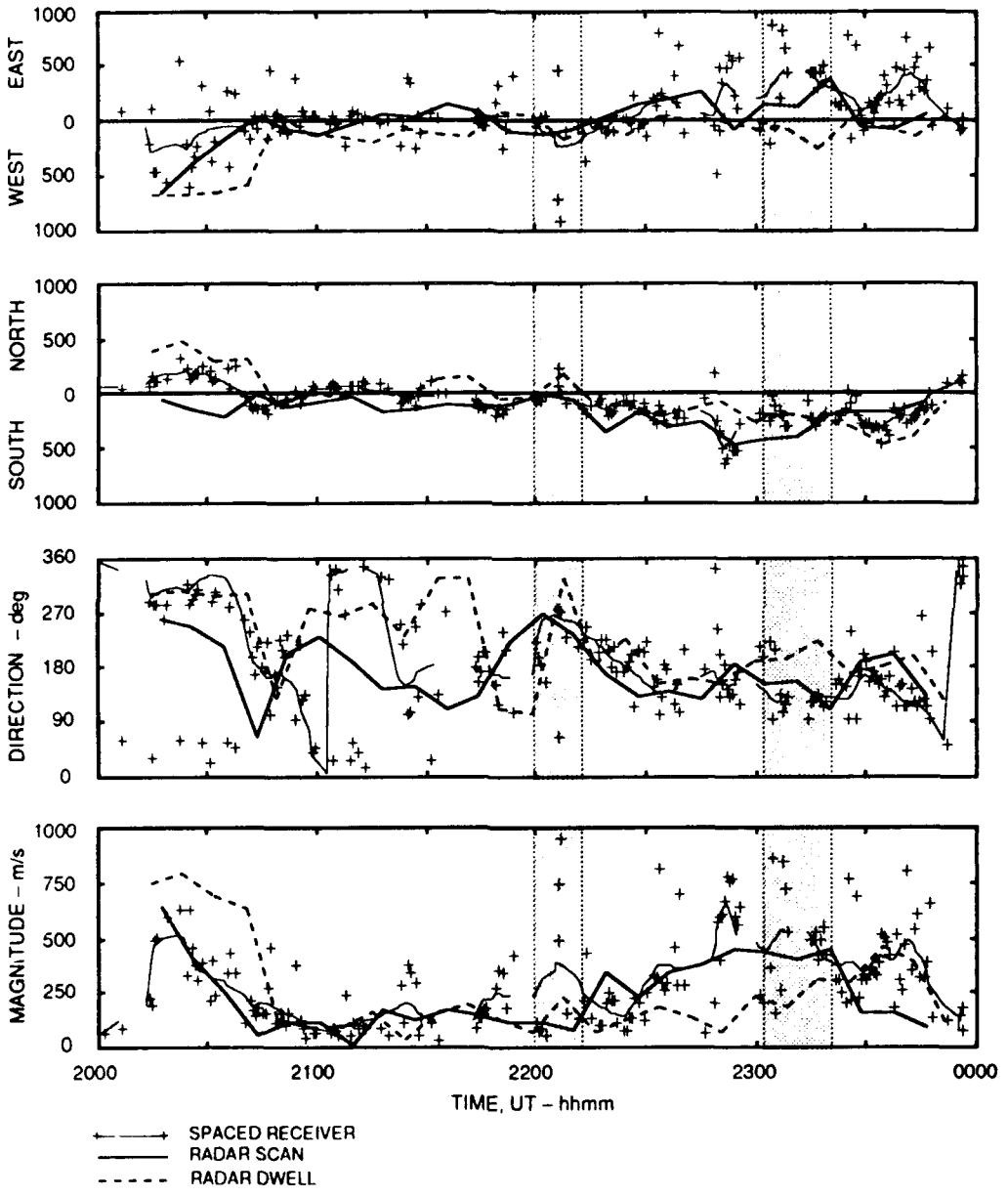

FIGURE 14 COMPARISON OF IRREGULARITY VELOCITY MEASURED BY SPACED-RECEIVER AND LARGE-SCALE PLASMA DRIFTS MEASURED BY RADAR SCANS AND DWELLS DURING 22 MARCH 1988 EXPERIMENT

This in turn suggests that the higher spatial resolution scan data are most appropriately compared to the spaced-receiver data (where the agreement is good). Also noteworthy during this period are the individual spaced-receiver velocity estimates, which are large but apparently counter-streaming to the westward flow. Conceivably, these could be caused by a velocity shear along the line of sight to the satellite, because of the integrated nature of the scintillation measurement. However, there is no suggestion in the radar data that drifts are eastward at any altitude. Therefore, these are most likely a product of incorrect extraction of pattern anisotropy from the data. As Figure 12 shows, the pattern is highly elongated for some samples during this time, which makes the numerical sensitivity of the velocity extraction difficult.

Between about 2100 UT and 2130 UT, the velocity magnitudes become small and there is a discrepancy between the spaced-receiver and radar-derived westward drifts. This is most obvious in the drift direction frame. This is also a period when the scintillation is weak, and the spaced-receiver data may be affected by temporal decorrelation of the ionospheric irregularities; that is, the correlation pattern is not temporally "frozen" as it slowly drifts through the antenna array. As a practical matter, however, the discrepancy between these and the radar data are well within the error bars of both measurement techniques.

Figure 14 shows good agreement between the radar and spaced-receiver velocities throughout most of the remainder of the experiment. The three exceptions are the conspicuous southeastward excursion in the spaced-receiver data near 2250 UT and the two periods that are shaded. Figure 12 shows that the excursion occurs just on the boundary of a structured region and that the correlation ellipse orientation deviates from the rod model. At this same time, there is also a sudden decrease in the peak density and layer altitude (which is not obvious in Figure 11), which can be interpreted as a parcel of ionization moving into the radar field of view from the north. The origin of the excursion therefore appears to be geophysical.

The two shaded regions in Figure 14 correspond to passages of a convection boundary overhead of the radar. These can be identified in the radar data line-of-sight velocities during the azimuth scans; they appear as significantly opposite flows at azimuth positions separated by only a few tens of degrees. The spaced-receiver data provide a single horizontal measurement with high time resolution of the detailed motion of the irregularities during the passage of the boundary. On the other hand, it is likely that the fixed-point radar dwells might sample a mix of spatially non-uniform line-of-sight velocities from either side of the convection boundary and indicate an erroneous large-scale bulk velocity. We can use the line-of-sight velocities observed during the passage of the boundary near 2315 UT and to illustrate how the radar dwell data can in error.

During the 2315 UT boundary passage, the discrepancy between the measured velocities in Figure 14 is primarily in the east-west component. That derived from the

radar fixed dwells has a moderate westward component, while the spaced-receiver drifts are larger and primarily eastward. Figure 15 shows the line-of-sight velocities during the azimuth scan at this time, as measured at each Doppler range gate of the radar. At most azimuth headings, there are seven range gates; those missing have very large error bars associated with the measurement of the Doppler shift. Because the radar elevation angle is 60°, the velocities are a function of both range from the radar and altitude. To the southeast at the time of this azimuth scan, the velocities have a large westward component: at Gate 5 (320-km altitude) the velocity exceeds 500 m/s. To the northeast of the radar, measured about 30 s later, the velocities are of similar magnitude, but have a strong eastward component. The positions of the fixed dwells are also indicated in Figure 15. One can see how resolution of the line-of-sight velocities under these circumstances might produce erroneous results.

D. Søndre Strømfjord, Greenland, 23 March 1988

On 23 March 1988, the previous day's experiment was repeated. The radio beacon satellite was approximately 5 min advanced in its orbit, leaving the propagation geometry effectively unchanged.

The resolved radar velocities from the azimuth scans on this evening are shown in Figure 16. The velocity pattern is generally more complex than on 22 March. Figure 17 shows the fixed-dwell-position-resolved velocities as a function of altitude and time. It is clear that there are some rapid changes in velocity magnitudes and directions throughout the evening. Figure 18 shows that the evolution of the electron-density profiles with time are similar to 22 March.

Figure 19 superimposes the radar data from both the fixed dwells and the azimuth scans on the spaced-receiver observations. The velocity magnitudes from the two radar measurements and the spaced-receiver measurement agree quite closely through the entire experiment. The velocity direction among the three techniques is also good between about 2030 UT and 2200 UT. For the periods before and after, the agreement is again better between the spaced-receiver data and azimuth-scan-resolved velocities than for the fixed-dwell radar data.

The spaced-receiver and radar data disagree significantly during the one period in the shaded portion of Figure 19. This corresponds to the passage of a convection boundary, similar to those seen in the 22 March data. The line-of-sight velocity pattern in Figure 20 indicates why the radar resolves a velocity that may well be erroneous. The dwells taken just before the scan might estimate the plasma velocity as strongly south-westward, while the spaced-receiver raypath measured eastward drift.

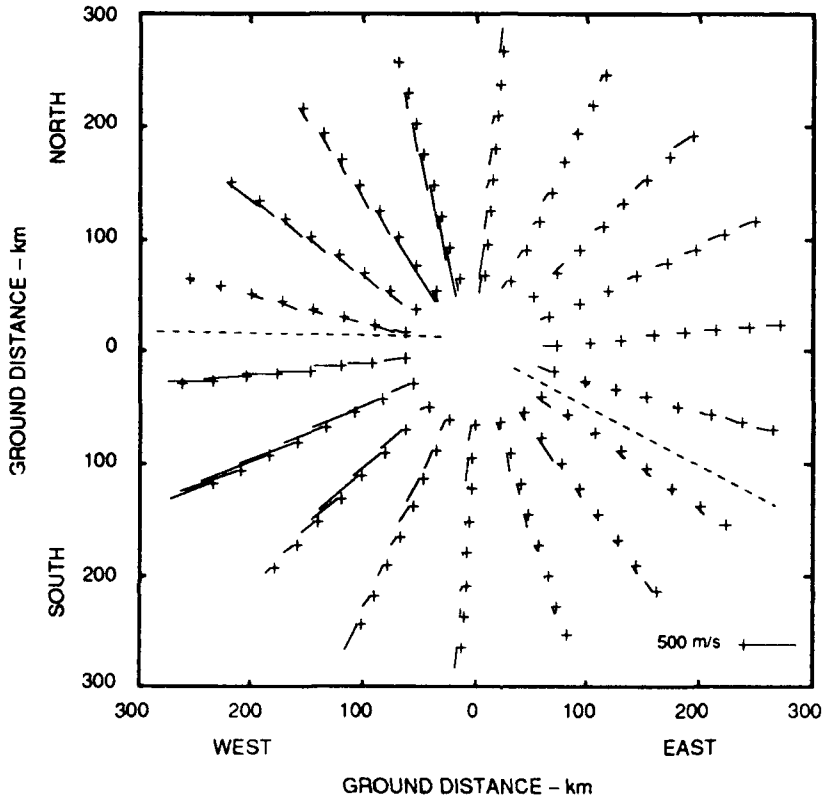

FIGURE 15 LINE-OF-SIGHT VELOCITY FROM A RADAR SCAN DURING 22 MARCH 1988 EXPERIMENT

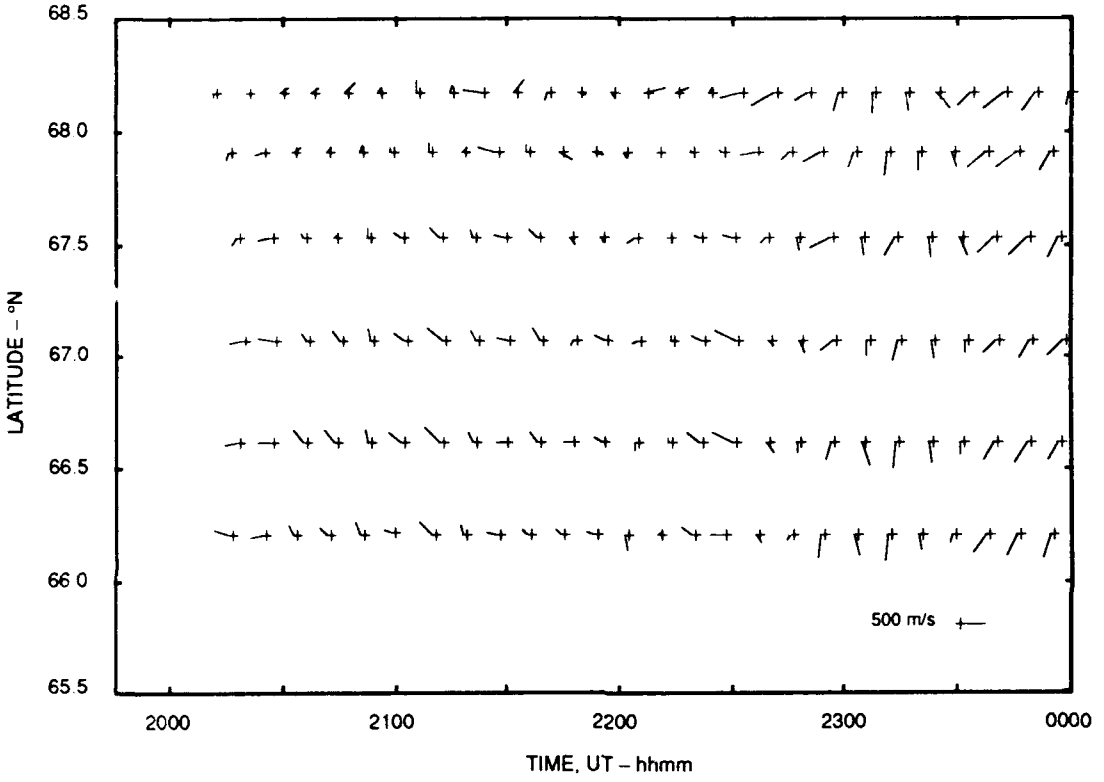

FIGURE 16 PATTERN OF VELOCITY AT AN ALTITUDE OF 270 km RESOLVED FROM RADAR SCAN DATA DURING 23 MARCH 1988 EXPERIMENT

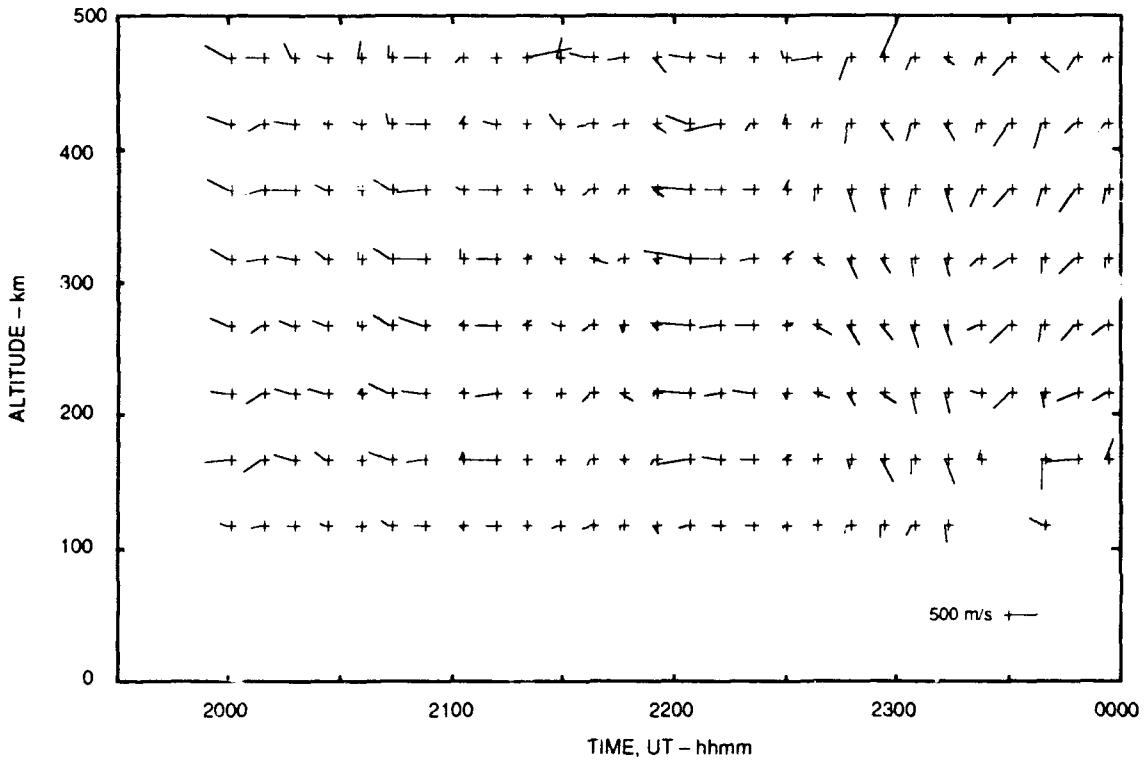

FIGURE 17 ALTITUDE PATTERN OF VELOCITY RESOLVED FROM MULTIPOSITION DWELLS DURING 23 MARCH 1988 EXPERIMENT

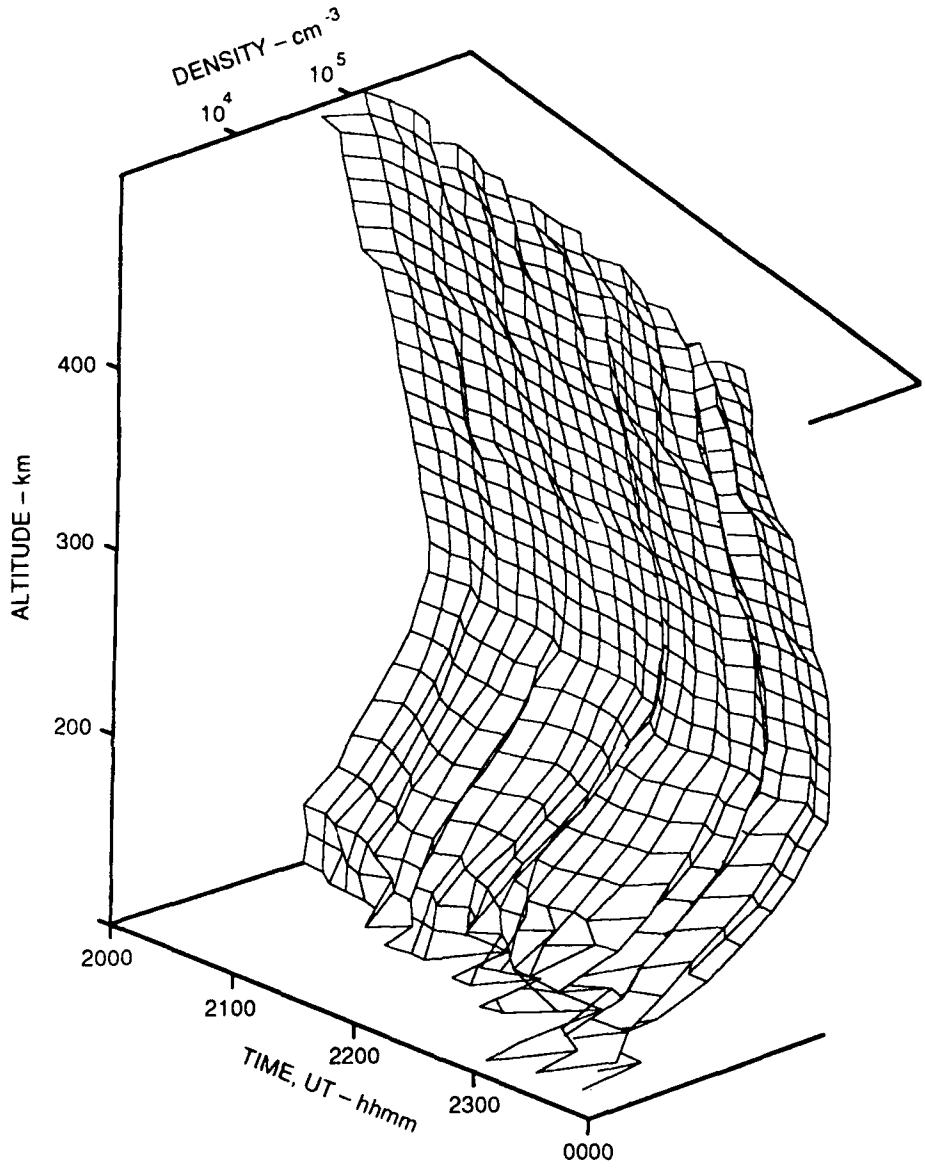

FIGURE 18 ELECTRON DENSITY PROFILES DURING 23 MARCH 1988 EXPERIMENT

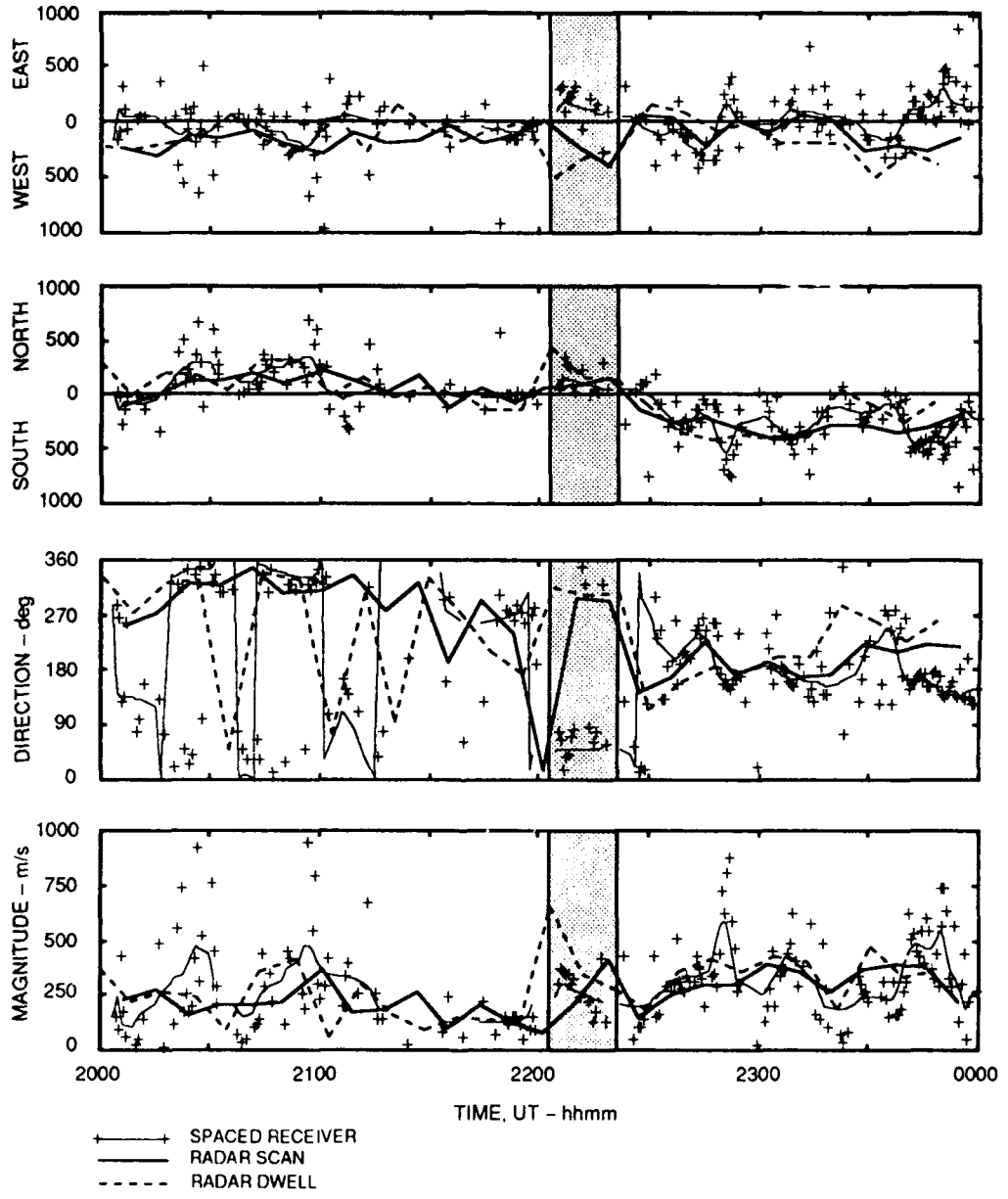

FIGURE 19 COMPARISON OF IRREGULARITY VELOCITY MEASURED BY SPACED-RECEIVER AND LARGE-SCALE PLASMA DRIFTS MEASURED BY RADAR SCANS AND DWELLS DURING 23 MARCH 1988 EXPERIMENT

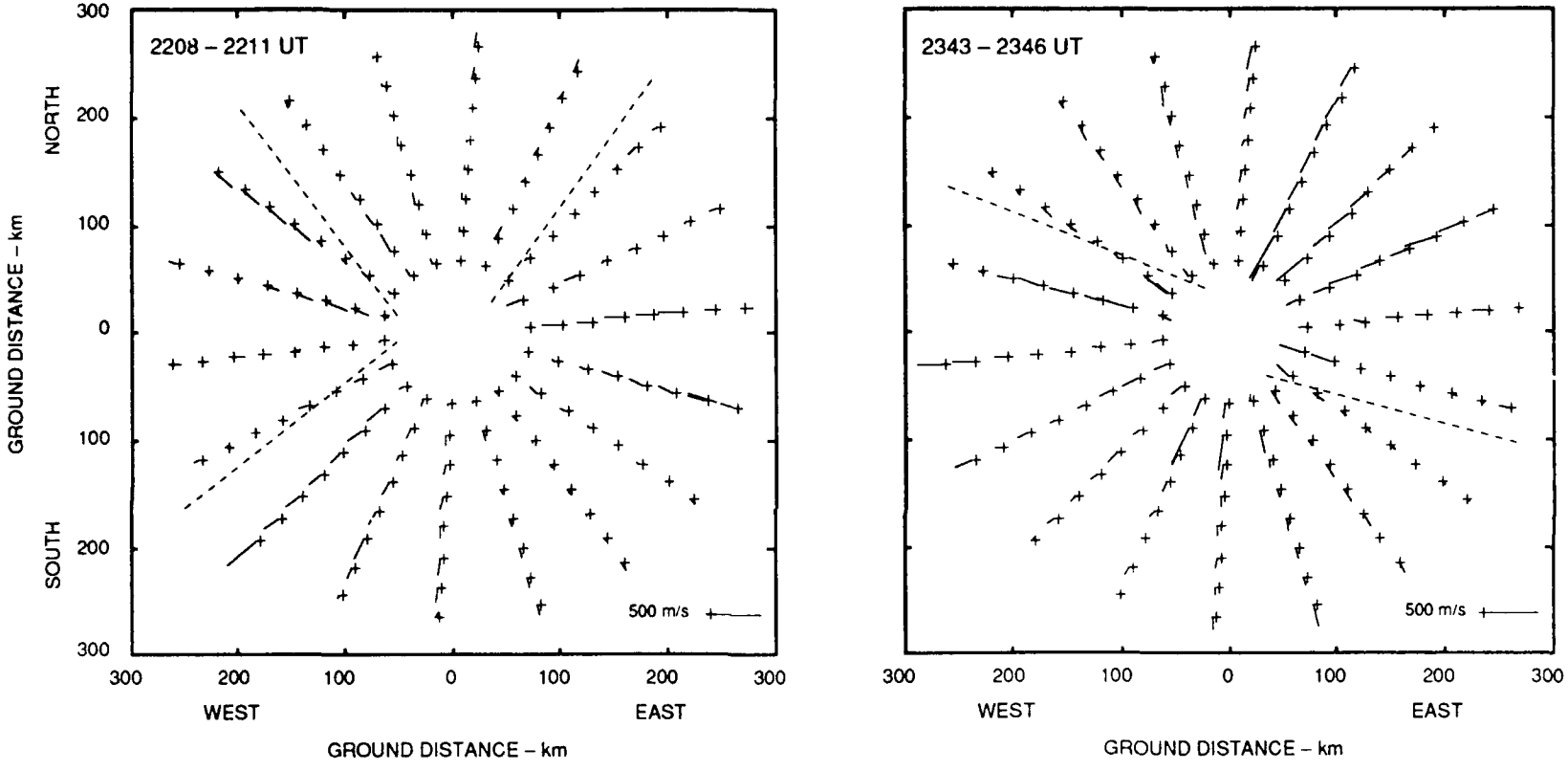

FIGURE 20 LINE-OF-SIGHT VELOCITY FROM RADAR SCANS DURING 23 MARCH 1988 EXPERIMENT

The next azimuth scan in the sequence, starting at 2216 UT, shows a similar but even more complex pattern of line-of-sight velocities with both eastward and westward components. It is inevitable that the radar Doppler samples (which are of necessity taken over such a large spatial area) can produce erroneous plasma-motion estimates when combined under an assumption of uniform drift.

Between 2230 and the end of the experiment at 0000 UT, the convection velocities are large, and vary significantly in latitude and time. The spaced receiver and radar scan velocities agree well until about 2330 UT, when they diverge. Figure 20(b) shows the line-of-sight velocities at 2345 UT and indicates the presence of another convection-reversal boundary. The radar scan velocities are resolved from an eastward-looking sector and are dominated by the westward drifts seen to the north. The azimuth of the spaced-receiver raypath at this time is slightly southeastward, where the drift is eastward, as the spaced-receiver data indicate.

E. Søndre Strømfjord, Greenland, 25 March 1988

The final experiment comparing spaced-receiver irregularity drifts with plasma motion measured by the radar was carried out early in the morning, local time, on 25 March 1988. During the time period 0430 UT through 0700 UT, a satellite beacon was at a high elevation angle (70°) to the east (90° 110° azimuth) of Søndre Strømfjord. Thus, the propagation geometry was very similar to the evening experiments on 22 and 23 March.

The analysis of the radar data from this experiment, and the comparisons with the spaced-receiver system are complicated by low F-region ionospheric electron density throughout much of the experiment and the appearance of a strong E layer at about 0715 UT. The first factor reduces the radar signal-to-noise ratio, and thus the measurement accuracy of Doppler shifts. Figure 21 shows the temporal variations of the electron profiles. The F-region densities are about 8×10^4, or about one-third those during the 22-23 March experiments. This results in a received signal-to-noise ratio that is generally inadequate to obtain useful resolved velocity vectors from the rapid azimuth scans. Although resolved velocities can be obtained from the dwells (because of the longer integration time), the error bars on these velocities tend to be high. It is important to note that the low electron-density levels *per se* are not a problem for the spaced-receiver measurements. A few percent perturbation of even these low background electron densities is enough to produce measurable intensity scintillation.

The comparison between the spaced receiver and radar data from the fixed dwells is shown in Figure 22. At first glance, the agreement appears to be poor. As with the nighttime data, the spaced receiver north-south component tends to be approximately the same magnitude as the radar-measured drifts.

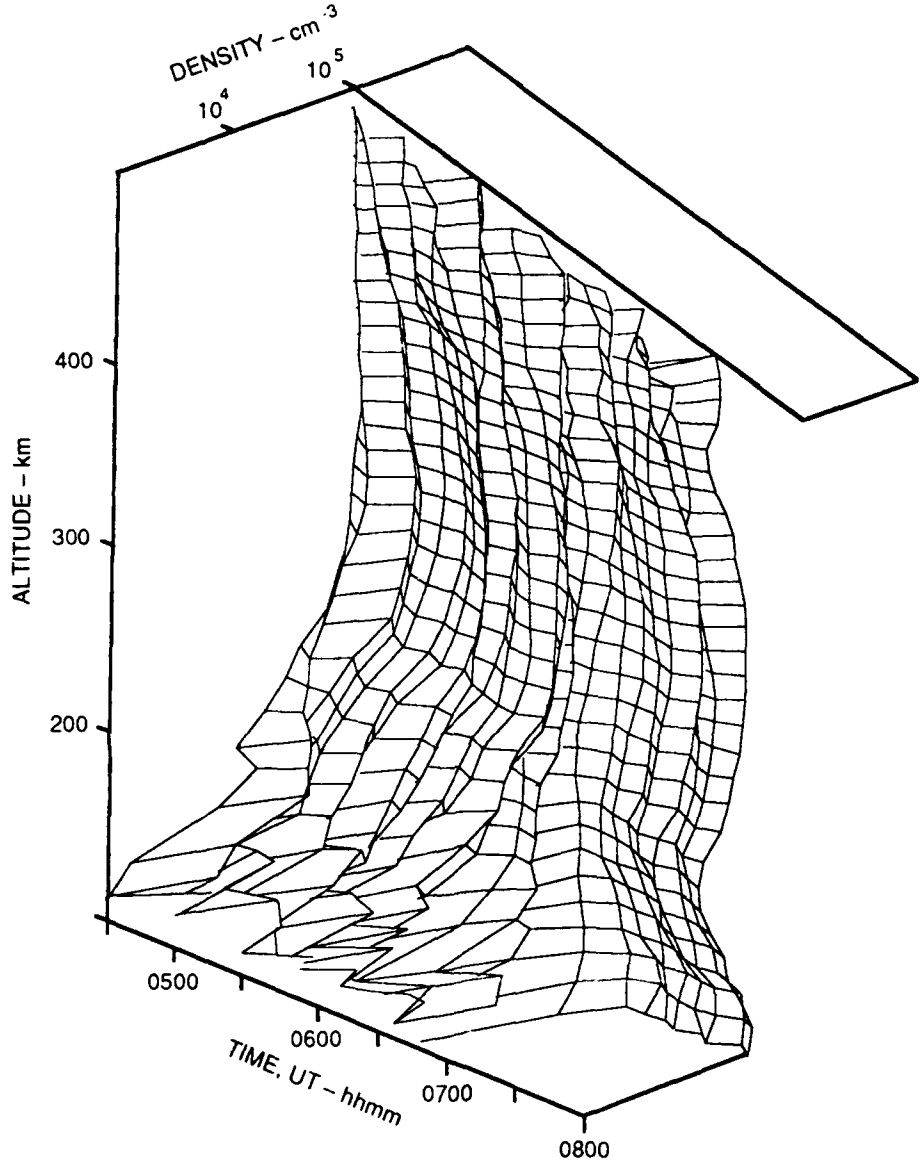

FIGURE 21 ELECTRON DENSITY PROFILES DURING 25 MARCH 1988 EXPERIMENT

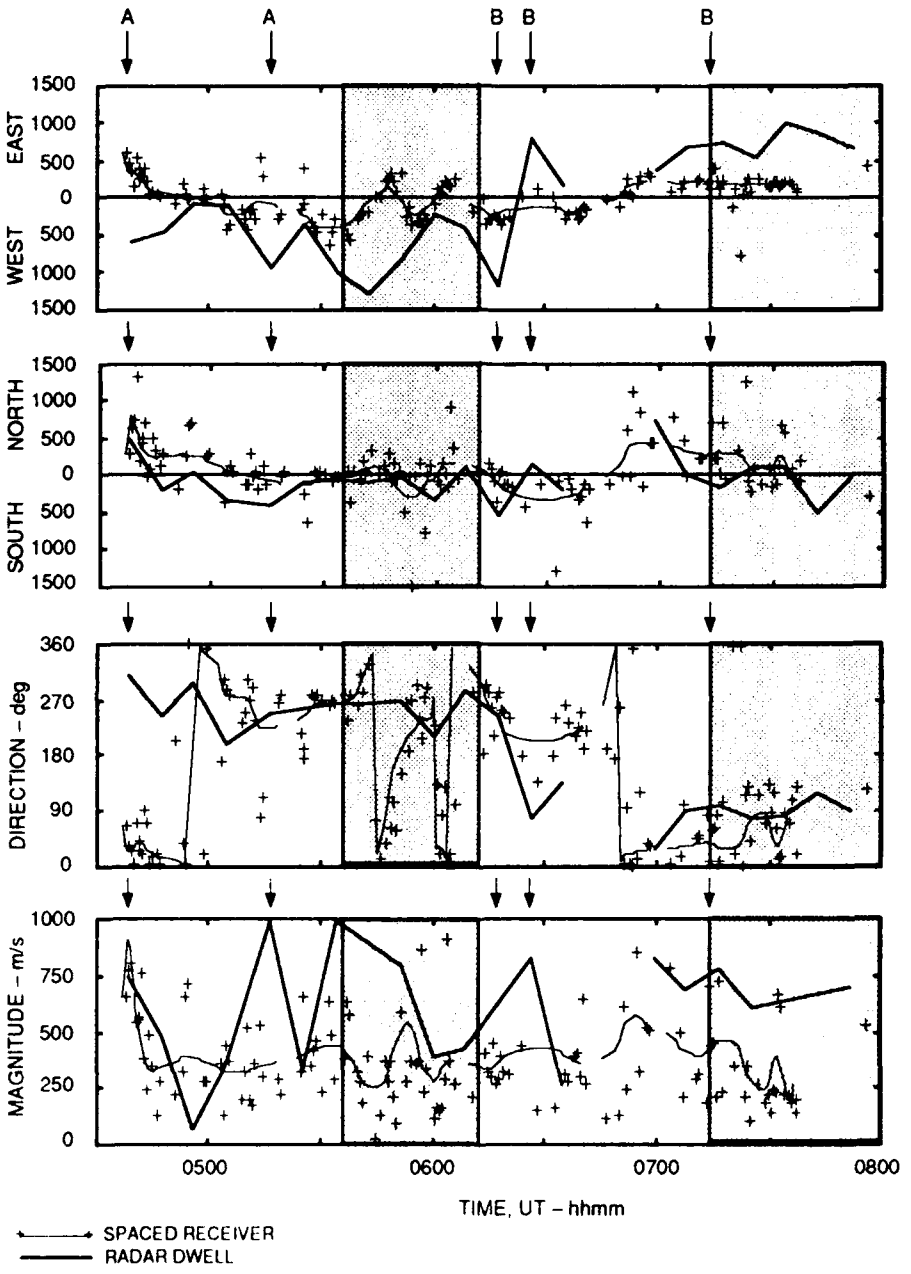

FIGURE 22 COMPARISON OF IRREGULARITY VELOCITY MEASURED BY SPACED-RECEIVER AND LARGE-SCALE PLASMA DRIFTS MEASURED BY RADAR DWELLS DURING 25 MARCH 1988 EXPERIMENT

However, the corresponding east-west derived velocities are generally much smaller than those derived by the radar and in places are of the opposite sign. Some of these discrepancies can be explained in terms of the complexity of the ionospheric dynamics and spatial smearing in the radar measurements. Other radar data are from very low electron density regions, and the confidence in the derived velocities is low. However, the differences between the techniques point out some particularly interesting features, that relate to ionospheric and magnetospheric electrodynamics.

From the beginning of the experiment, two points have been labeled "A": one shortly after 0430 UT and one at about 0520 UT. Based on the line-of-sight radar data from the fixed positions and the scans (which is of moderate quality for this period), these are velocities from regions of complex dynamics. The line-of-sight patterns for 0443 UT and 0520 UT are shown in Figure 23, where the circles are the scan data and the squares are the dwell data. Note that data from a number of gates are missing because of the low electron density and signal-to-noise ratio. The 0443 UT data are generally chaotic; the 0520 UT patterns show the passage of a flow reversal boundary. The data plotted in Figure 22 are from the fixed dwells, and it is possible to see how the resolution of those line-of-sight samples results in a vector that is generally southward. However, the scan data point out how nonuniform the drift is. In fact, in the direction of the satellite raypath (slightly south of east), the drifts have only a weak southward component, consistent with the spaced-receiver data.

Two additional points in Figure 22 have been labelled as "B"; these are velocities from regions of very low electron density. The 10-s integration scan data during this period produce only a handful of random points: therefore, there is little useful line-of-sight data. Unfortunately, little can be said about the discrepancy between the very large plasma drifts and the spaced-receiver data. The quality of the radar data is distinctly in question, however.

The two shaded portions of Figure 22 are the most interesting parts of the radar/spaced-receiver comparison for this experiment. The first period (approximately 0500 to 0600 UT) is of interest because of the velocity pattern observed in the spaced-receiver data. The line-of-sight velocities from the scans are chaotic during this time and show multiple flow reversals. The general conclusion is that there is velocity structure passing overhead of the radar, which the fixed dwells cannot resolve spatially. The spaced-receiver data show a pattern of rotation and velocity magnitude that is quite consistent; this is particularly clear in the velocity direction pattern. When plotted as a time-space pattern, these data produce the skewed dual vortex pattern shown in Figure 24. This is an intriguing result, in that this is the local time at which similar patterns have been implied from the Greenland magnetometer chain data (Friis-Christensen et al., 1988), and attributed to flux transfer events. It is impossible to say with these data alone, that the spaced-receiver velocity pattern we observe is from such an event. However, it does point out the potential of measuring such events, which have structure that is difficult to resolve by the standarad radar scanning technique.

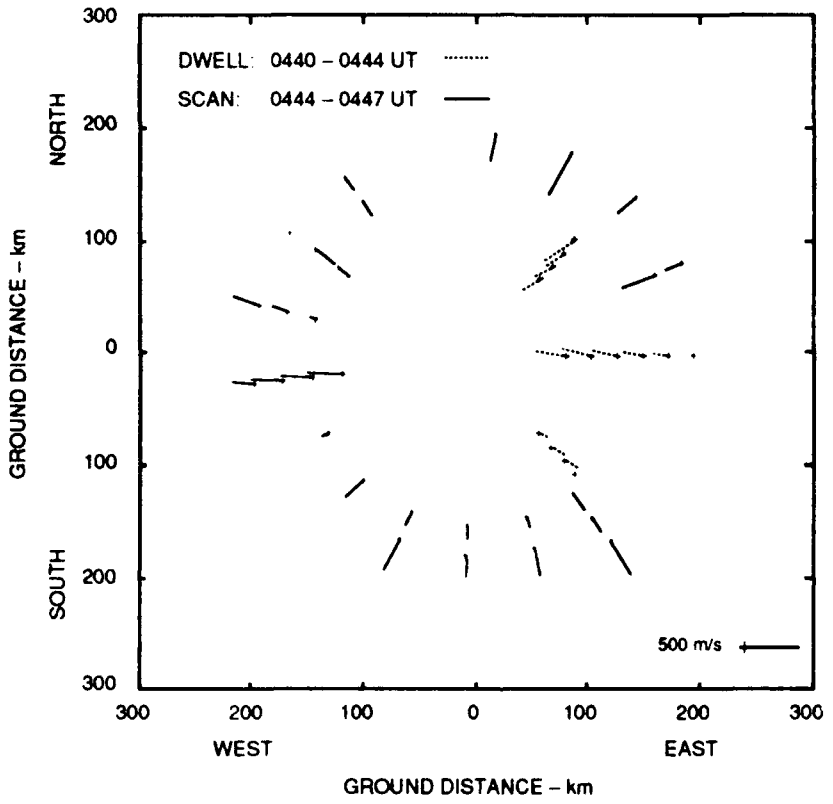

FIGURE 23 LINE-OF-SIGHT VELOCITIES FROM A RADAR SCAN AND THE SUBSEQUENT DWELL DURING 25 MARCH 1988 EXPERIMENT

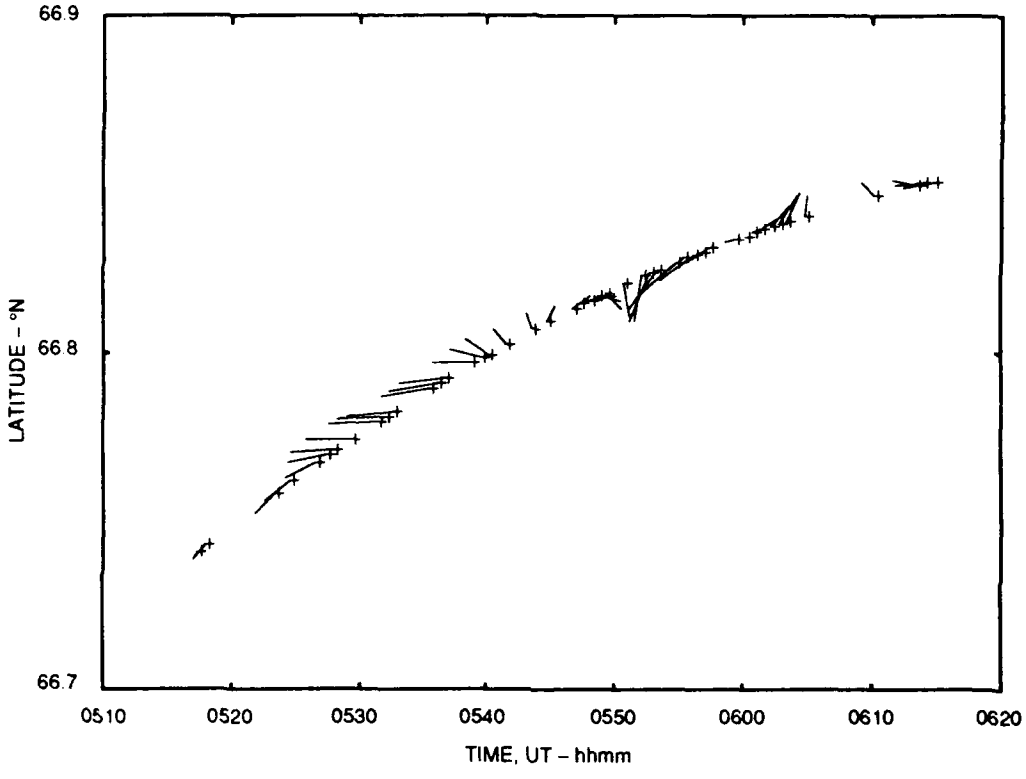

FIGURE 24 PATTERN OF VELOCITY AT AN ALTITUDE OF 270 km RESOLVED FROM RADAR SCAN DATA DURING 22 MARCH 1988 EXPERIMENT

The second shaded area in Figure 22 is interesting in another way. This is the region where an E layer has appeared with peak density the same or greater than the F layer. The spaced-receiver east-west velocity component is significantly smaller than those from the radar scans. In this case, the velocity discrepancy cannot be attributed to a complex velocity pattern. The line-of-sight velocities for this period imply a relatively consistent flow pattern, consistent with the dwell data. It is more likely that the spaced receiver is measuring the motion of irregularities in the upper E layer, rather than the F layer. During this period, the integrated plasma content of the E region exceeds that of the F layer; under that condition, the scintillation statistics will be dominated by structure at lower altitudes. It seems likely that the consistently lower irregularity velocity measured by the scintillation technique is that of low-altitude irregularities, and reflects the slow, rotated, E region Pedersen drifts.

V CONCLUSIONS

We have compared simultaneous observations of high-latitude ionospheric motion measured using two techniques, incoherent scatter radar and spaced-receiver scintillation. The incoherent scatter radar determines the bulk plasma drift, while the scintillation measures the motion of kilometer-scale irregularities embedded within the plasma. The radar can unambiguously determine line-of-sight Doppler shifts in any direction and altitude, but must use angularly separated collection of these to resolve a velocity vector. Thus, its temporal and spatial resolution is relatively poor. The spaced-receiver technique measures the integrated scattering effects along an transionospheric path and is therefore subject to ambiguity. On the other hand, the scintillation measurement determines the motion at a single horizontal point in the ionosphere and can have time resolution as good as a few tens of seconds.

When the ionospheric motion is uniform or slowly changing, the agreement between the two methods is good. At other times, when there is velocity structure overhead, the resolved radar vectors can be incorrect. This is because the line-of-sight components used to resolve the vector are inconsistent; our examples have shown specifically that this is the case. Unfortunately, the data used here were not processed to provide rigorous error bars, which would be useful in the detailed comparisons.

The path integration effects, which are the main concern with the spaced-receiver data, appear to be less significant than expected. Evidence of this is that there are only a few periods in the examples we have shown where discrepancies with the radar data cannot be explained. The strength of the spaced-receiver technique is the excellent temporal and spatial resolution; in the data one can see structure on the convection-reversal boundaries, which is well below the resolution of the radar.

The examples point out some conditions (e.g., very low drifts, a conducting E layer) that will affect the behavior of the scintillation-producing irregularities and thus the interpretation of the spaced-receiver data. These specific effects might best be studied in additional coordinated observations with the Søndre Strømfjord radar.

One of the purposes of this report was to determine the potential of the spaced-receiver method as a means to routinely monitor ionospheric motion at high latitudes. We have shown that such a system would be useful, particularly if an array of stations distributed at high latitudes could be used.

VI REFERENCES

Armstrong, J.W., and W.A. Coles, 1972: "Analysis of Three Station Interplanetary Scintillation," *J. Geophys. Res.*, Vol. 77, pp. 4602-4610.

Basu, Su., S. Basu, E. Costa, C. Bryant, C.E. Valladares, and R.C. Livingston, 1991: "Interplanetary magnetic field control of drifts and anisotropy of high-latitude irregularities," *Radio Sci.*, Vol. 26, pp. 1079-1103.

Briggs, B.H., 1968: "On the Analysis of Moving Patterns in Geophysics, I, Correlation Analysis," *J. Atmos. Terr. Phys.*, Vol. 30, pp. 1777-1788.

Briggs, B.H., and I.A. Parkin, 1963: "On the Variation of Radio Star and Satellite Scintillations with Zenith Angle," *J. Atmos. Terr. Phys.*, Vol. 25, p. 339.

Cannon, P.S., B.W. Reinisch, J. Buchau, and T. Bullett, 1991: "Response of the Polar Cap F Region Convection Direction to Changes in the Interplanetary Magnetic Field: Digisonde Measurements in Northern Greenland," *J. Geophys. Res.*, Vol. 96, pp. 1239-1250.

Costa, E., and P.F. Fougere, 1988: "Cross-Correlation Analysis and Interpretation of Spaced-Receiver Measurements," *Radio Sci.*, Vol. 23, pp. 141-162.

Evans, J.V., 1969: "Theory and Practice of Ionospheric Study by Thompson Scatter Radar," *Proc. IEEE*, Vol. 57, pp. 496-530.

Evans, J.V., 1972: "Ionospheric Movements Measured by Incoherent Scatter: A Review," *J. Atmos. Terr. Phys.*, Vol. 34, pp. 175-209.

Friis-Christensen, E., M.A. McHenry, C.R. Clauer, and S. Vennerstrom, 1988: "Ionospheric Traveling Convection Vortices Observed Near the Polar Cleft: A Triggered Response to Sudden Changes in the Solar Wind," *Geophys. Res. Lett.*, Vol. 15, pp. 253-256.

Greenwald, R.A., K.B. Baker, R.A. Hutchins, and C. Hanuise, 1985: "An HF Phased-Array Radar for Studying Small-Scale Structure in the High-Latitude Ionosphere," *Radio Sci.*, Vol. 20, p. 63.

Kelley, M.C., ed., 1990: A Polar Cap Observatory, (Cornell University, Ithaca, New York).

Livingston, R.C., C.L. Rino, J. Owen, and R.T. Tsunoda, 1982: "The Anisotropy of High-Latitude Nighttime F Region Irregularities," *J. Geophys. Res.*, Vol. 87, pp. 10,519-10,526.

Livingston, R.C. and T.M. Dabbs, 1986: Phase Scintillation Under Weak and Strong Scatter Conditions, DNA-TR-86-001, Defense Nuclear Agency.

Mitra, A.N., 1949: "A Radio Method of Measuring Winds in the Ionosphere," *Proc. IEEE*, Vol. 96, pp. 441-446.

Rino, C.L., 1979: "A Power-Law Phase Screen Model for Ionospheric Scintillation, 1, Weak Scatter," *Radio Sci.*, Vol. 14, pp. 1135-1140.

Rino, C.L., 1982: "On the Application of Phase Screen Models to the Interpretation of Ionospheric Scintillation Data," *Radio Sci.*, Vol. 17, pp. 855-867.

Rino, C.L., and R.C. Livingston, 1982: "On the Analysis and Interpretation of Spaced-Receiver Measurement of Transionospheric Radio Waves," *Radio Sci.*, Vol. 17, pp. 845-854.

Tsunoda, R.T., 1988: "High-Latitude F Region Irregularities: A Review and Synthesis," *Rev. Geophys.*, Vol. 4, pp. 719-760.